Magnetic and structural phase transitions of multiferroic boracites $M_3B_7O_{13}X$ (M = 3d transition metal Cr–Zn or Mg; X = halogen Cl, Br, I)

Walter Schnelle*
Max-Planck-Institut für Chemische Physik fester Stoffe, Nöthnitzer Straße 40, 01187 Dresden, Germany

Hans Schmid†
Université de Genève, Département de Chimie minérale, analytique et appliquée, 30, quai Ernest-Ansermet, 1211 Genève 4, Switzerland
(Received 7 November 2014; revised manuscript received 24 February 2015; published 20 May 2015)

The specific heat capacity of mostly single-crystalline samples of 21 boracite compounds $M_3B_7O_{13}X$ with M a 3d transition metal (Cr, Mn, Fe, Co, Ni, Cu, Zn) or Mg and X a halogen (Cl, Br, I) is determined. In combination with magnetic susceptibility data the magnetic ordering of the M^{2+} ions at T_N is investigated in detail. The fully ferroelectric/fully ferroelastic structural phase transitions at higher temperatures are measured by differential scanning calorimetry. In the Cr-Br, Cr-I, Cu-Cl, and Cu-Br compounds, previously unknown magnetic phases were found. Magnetic order in the boracites is characterized by the quantum and classical spin states of the M^{2+} ions, a variable degree of structural distortion, orbital effects, and competing exchange interactions. The Cu-Cl, Cu-Br, and Ni-Cl boracites exhibit broad maxima of magnetic specific heat and of magnetic susceptibility above T_N caused by low-dimensional or frustrated magnetic interactions. Co boracites display additional broad anomalies below T_N originating from continuous spin reorientations and effective $S = 1/2$ ground states. Indications for spin reorientations are also observed for Fe boracites. New phases appear in high magnetic fields for some Co and Fe boracites, which is not the case for the Mn compounds. Stronger magnetic frustration is deduced for the cubic Cr compounds. For the latter compounds and Ni-I boracite magnetostructural phase transitions are observed.

DOI: 10.1103/PhysRevB.91.184411 PACS number(s): 75.40.Cx, 77.84.−s, 75.80.+q, 61.50.Ks

I. INTRODUCTION

In 1787, a new mineral, "cubic quartz" from Lüneburg in northern Germany, was described [1], which little later turned out to be a magnesium halogenoborate and baptized "Borazit" by Werner [2,3]. Its most peculiar physical property, "electricity" (pyroelectricity), was discovered already in 1791 by Haüy [4]. Boracite was among the minerals for which piezoelectricity was originally described [5]. The boracite family of compounds [6] comprises today a great variety of synthetic homologues [7–11] as well as a number of minerals [12–17].

The magnesium and 3d-transition-metal boracites are compounds with the general formula $M_3B_7O_{13}X$, where M stands for the divalent cation of Mg, Cr, Mn, Fe, Co, Ni, Cu, Zn, and Cd, and X for the monovalent anion of OH, F, Cl, Br, I, or NO_3. If the monovalent anion is replaced by the divalent anion of the chalcogenides Q = S, Se, or Te, the structure is characterized by oxygen vacancies, resulting in the formula $M_3B_7O_{13-\delta}Q$ [18]. The $Li_4B_7O_{12}X$ (X = Cl, Br, I) [19] and $Li_5B_7O_{12}Q$ compounds have structures closely related to the $M_3B_7O_{13}X$ boracites. Whereas the Li-X compounds are ionic conductors, the Mg and transition-metal oxoboracites are transparent insulators. Recently, the synthesis and properties of new Fe-OH boracites have been reported [20–22].

Following the discovery of simultaneous ferroelectricity and weak ferromagnetism in nickel iodine boracite $Ni_3B_7O_{13}I$ [23–25]—the first material in which the spontaneous magnetization was switched by an electric field and the spontaneous polarization by a magnetic field—the group of 3d-transition-metal boracites has attracted particular interest in the past fifty years. The major reason was that in 1894 P. Curie conjectured on symmetry grounds that materials might exist which could be polarized electrically by means of a magnetic field and magnetized by means of an electric field [26]. It took more than fifty years until such effects were indeed found in crystals (for overviews see Refs. [27–40]). Today, essentially three kinds of such effects are distinguished in single phase materials, all of which are for symmetry reasons allowed in the ferroelectric (FE)/ferromagnetic (FM)/ferroelastic (FEla) phases of the M-X boracites [36,41].

(1) The linear magnetoelectric (ME) effect, characterized by the term $\alpha_{ik}E_iH_k$ in the free enthalpy, and permitting the induction of a polarization P by means of a magnetic field H, $P_k = \alpha_{ki}H_i$ (ME_H effect), or of a magnetization M by means of an electric field E, $M_k = \alpha_{ik}E_i$ (ME_E effect). For definitions, units, techniques, and information on the tensor α_{ik}, we refer to Refs. [36,42–44].

(2) The bilinear ME effects, characterized by the terms $\frac{1}{2}\beta_{ijk}E_iH_jH_k$ and $\frac{1}{2}\gamma_{ijk}H_iE_jE_k$ of the free enthalpy, permitting, for example, the induction of a polarization $P_k = \frac{1}{2}\beta_{kij}H_iH_j$ proportional to H^2, or the induction of a magnetization $M_k = \frac{1}{2}\gamma_{kij}E_iE_j$ proportional to E^2 [42].

(3) The switching by reorientation of the spontaneous magnetization M_i^s by means of an electric field and the 180° switching or reorientation of the spontaneous polarization P_i^s by means of a magnetic field. These two mutually converse effects require ferroelasticity in addition to simultaneous ferroelectricity and ferromagnetism. Ni-I boracite is so far the only boracite compound on which these effects have been demonstrated experimentally [23,24,45], but in many other M-X boracites these effects are symmetry-allowed, too [41,46] (cf. Table I).

*walter.schnelle@cpfs.mpg.de
†Deceased.

TABLE I. Different types of observed phase sequence in boracites $M_3B_7O_{13}X$ (M-X). The phases are given in Heesch-Shubnikov point group symbols. All transitions to or between magnetic phases are of second order, those between para- or diamagnetic phases are of first order. FM = ferromagnetic, AFM = antiferromagnetic, FE = ferroelectric, FEla = ferroelastic. (?) after composition M-X means that the given magnetic point group is probable, but not yet verified. The magnetic phase of Cu-I has not yet been investigated.

cubic		tetragonal	orthorhombic	monoclinic	rhombohedral	orthorhombic			monoclinic	triclinic	
paraelectric		full FEla	full ferroelectric (FE) / full ferroelastic (FEla)								boracite compounds M-X
prototype							ferromagnetic (FM)				M = Mg, Cd or 3d-metal ions
para- or diamagn.	AFM	para- or diamagnetic				AFM	partial	full	partial	full	X = F, Cl, Br, I, OH or NO_3
$\bar{4}3m1'$	$\bar{4}3m$[b] or $\bar{4}'m3'$[b]										Cr-Br(?), Cr-I(?)
$\bar{4}3m1'$			(phase transition(s) not yet known, probably analogous to Cr-Br and Cr-I)								Cu-I
$\bar{4}3m1'$									m'[c]		Ni-I
$\bar{4}3m1'$			$mm21'$								Mg-Cl/Br/I(?), Zn-Br/I, Zn-NO_3[a] Cd-Cl/Br/I/NO_3[a] Ni-Cl/NO_3[a]
$\bar{4}3m1'$			$mm21'$					$m'm2'$[c]			Co-Br/I/NO_3[a]
$\bar{4}3m1'$			$mm21'$					$m'm2'$[c]		1[c]	Ni-Br
$\bar{4}3m1'$			$mm21'$			$mm2$[c]	$m'm'2$[b]				Cu-Cl/Br
$\bar{4}3m1'$		$\bar{4}2m1'$	$mm21'$			$mm2$[c]	$m'm'2$[b]				Cr-Cl
$\bar{4}3m1'$			$mm21'$				$m'm'2$[b]				Mn-I, Cu-NO_3[a]
$\bar{4}3m1'$			$mm21'$	$m1'$	$3m1'$						Zn-Cl
$\bar{4}3m1'$			$mm21'$	$m1'$	$3m1'$				m[c]		Co-Cl, Fe-I/Cl(?)
$\bar{4}3m1'$			$mm21'$		$3m1'$				m[c]		Fe-Br(?)
$\bar{4}3m1'$					$3m1'$				m[c]		Co-F(OH)[a]
$\bar{4}3m1'$					$3m1'$						Mg-OH/F, Zn-F

[a]The prototype $\bar{4}3m1'$ is only hypothetic because the compound M-X decomposes before transforming to $\bar{4}3m1'$.
[b]Ferrotoroidicity not allowed.
[c]Ferrotoroidicity allowed.

In addition to these ME effects, a spontaneous *toroidal moment* T_i^s is allowed in several magnetic phases of the M-X boracites (see Table I). For reviews on toroidal moments see Refs. [47–51] and for a thorough theoretical analysis Ref. [52]. There exist 31 Heesch-Shubnikov point groups allowing a spontaneous polarization P_i^s (a polar vector), 31 a spontaneous magnetization M_i^s (an axial vector), and 31 a spontaneous toroidal moment T_i^s, an axio-polar (time-odd polar) vector [53]. Among the 13 groups allowing both P_i^s and M_i^s, 9 allow T_i^s, too. Because many ferroelectric/ferromagnetic phases of boracites belong to groups permitting T_i^s, they are candidates of utmost interest for the study of this so far little known axiopolar vector moment in crystals [54–59]. The additional occurrence of ferroelasticity, characterized by the symmetrical second rank tensor spontaneous deformation ${}^s\epsilon_{ik}$, requires a nonequiphase transition from the high-temperature prototype phase to a ferroic phase.

The scientific importance of the 3d transition-metal boracites also resides in the fact that several magnetically ordered phases of which represent *ideal multiferroic model substances* with the highest possible number of primary ferroic properties. Multiferroics [37,38,60–65]—a field of condensed matter physics which has seen a vigorous resurgence of interest in the last decade [64]—were originally defined as materials allowing the simultaneous presence in the same phase of two or more of the primary ferroic properties: *ferroelectricity* (FE), (weak) *ferromagnetism* (FM), and *ferroelasticity* (FEla) [41]. Later, *ferrotoroidicity* (FTo) was proposed as a fourth primary ferroic [34,36,47,50], characterized by a toroidal moment changing sign both under space and time reversal. According to a recent classification of multiferroics [65], comprising also antiferromagnetic ferroelectrics, boracites belong to type-I, i.e., polarization and magnetic order are of different origin (nuclear structure/spin structure), whereas in type-II multiferroics they are of same origin (spin structure only), leading to strong mutual coupling. In a variety of boracites and with different magnetic point groups (1, m, m', $m'm2'$), all four primary ferroic properties are allowed in the same phase (see Table I) and give rise to different cross-couplings. The symmetry properties of such materials can be classified following Ascher [23,53] using the parity operations of space and time, i.e., with respect to the four irreducible representations of the dihedral group $\bar{1}1'$ of order four (generated by $\bar{1}$ and $1'$), corresponding to identity E, space inversion $\bar{1}$, time reversal $1'$ and the product of both $\bar{1}'$ (Table II).

Ferrotoroidic domains [58] and their particular walls [59] have been predicted for boracites, however, it has been shown that such domains are necessarily always (weakly) ferromagnetic or antiferromagnetic, thus a new, independent type of domain is not created [40]. This is corroborated by the fact that when extending Aizu's concept of species of phase transitions [68] to ferrotoroidicity, the total number of species does not increase [69]. Consequently ferromagnetic/ferrotoroidic domains can be revealed, e.g., by spontaneous Faraday rotation (e.g., on Co-I) [40] and nonlinear optical effects [38]. In the polar, ferrimagnetic $Ga_{2-x}Fe_xO_3$, which has the same orthorhombic magnetic point group as several boracite compositions, the presence of a toroidal moment has been evidenced by a toroidal component of the linear ME effect [70]. Therefore it is likely that boracites will also show toroidal components of their spin structure. FE domain walls can give a noteworthy contribution, e.g., to the specific heat [71]. A high density of the very similar FEla walls can therefore also be expected to give contributions of the same order of magnitude. Analogously, anti-phase domain walls, FM, AFM, and FTo domain walls can be expected to give contributions, too. However, no experimental evidence has so far been reported nor obtained in the present study.

TABLE II. The four types of spontaneous primary ferroic quantities under the parity operations of space and time (see also Refs. [40,47,50,53,66,67]).

E	$\bar{1}$	$1'$	$\bar{1}'$	spontaneous quantity	ferroic order
1	1	1	1	deformation ${}^s\epsilon_{ik}$	ferroelasticity (FEla)
1	−1	1	−1	polarization ${}^sP_i$	ferroelectricity (FE)
1	1	−1	−1	magnetization ${}^sM_i$	ferromagnetism (FM)
1	−1	−1	1	toroidal moment ${}^sT_i$	ferrotoroidicity (FTo)

Nearly all M-X boracites are characterized by a sequence of structural phase transitions (PTs) from a cubic high-temperature (prototype) phase to FE/FEla phases, which order magnetically at low temperatures. Table I gives an overview of the various types of observed phase sequence, the phases being indicated in Heesch-Shubnikov point groups, and in Table III of Ref. [72] (containing Refs. [73–123]), the values of the transition temperatures and the magnetic space groups are collected.

The investigation of the low-temperature phases of boracites is a formidable task. Several methods are hampered by the presence of FE/FEla domains in the crystals. In cooling through the cubic → orthorhombic PT up to six such domains may be generated. Most crystal symmetry information therefore was obtained from optical studies on microscopically small single domains, prepared by *in situ* application of electrical fields or of uniaxial stress. In order to perform reliable structure refinements from x-ray diffraction data either single domain crystals have to be prepared (or need to be found) or one has to resort to powder methods. For a small number of distorted boracite phases the complete crystal structure including atomic positions is known. Moreover, the unit cells of boracite phases are large. They contain four formula units (96 atoms) with three inequivalent metal sites in the orthorhombic cells and twice as many in the cubic phases. Investigations of the magnetic structure by powder neutron diffraction have been done for a few species only since large samples with ^{11}B isotope are required.

Here, we present the results of a study of the low-temperature properties and of the magnetically ordered phases of 21 M-X boracite species by heat-capacity and magnetization measurements on multidomain crystals. The thermal properties at the FE/FEla structural PTs are also investigated. Our findings are discussed in conjunction with published phase symmetry information. Specific heat data have been reported for only few boracite species [76,124,125] while phase diagrams of boracites in high magnetic fields have not been explored at all. Here, we studied specific heat in fields up to 140 kOe [126] and find that the M-X boracites display a wealth of interesting magnetic phases. The compounds of the series feature both quantum spin (Cu^{2+}, Ni^{2+}) as

well as classical spin (Mn^{2+}) systems. The behavior of several boracites shows the influence of low-dimensional and frustrated magnetic exchange interactions of quite different origin. This is due to the widely variable degree of structural distortion found in these compounds. We here refrain from analyzing these interactions further, which is a future task for the more interesting boracite species. Instead, the work is intended to provide an overview on the relationship of structure and magnetism in the series.

The paper is organized as follows. In Sec. II, we describe our samples and measurement methods and an introduction to the crystal structure of the boracites is given in Sec. III. The methods for the analysis of the specific heat data are outlined in Sec. IV. Section V is devoted to results on nonmagnetic Mg-Cl and Zn-X (X = Cl, Br, I) boracites. In Secs. VI–XI, the data for Cu, Ni, Co, Fe, Mn, and Cr-X boracites discussed in detail. We close with a discussion of the dependence of the magnetic properties on the crystal structure (Sec. XII) and the summary and outlook.

In Ref. [72], our results on the structural PTs are presented. These PTs occur at temperatures well above the magnetic ordering, except for the boracite species in which coupled magnetostructural PTs are observed. The dependence of the transition enthalpy from the type of the structural changes and the influence of growth sectors on the cubic ↔ orthorhombic PT are discussed.

II. SAMPLES AND METHODS

The Mg-Cl and the M-X boracites were synthesized by chemical transport reactions [99,100]. The samples used for the magnetization and calorimetric measurements were intensely colored (apart the Mg-Cl and Zn-X species) multidomain crystals of largely varying size and shape (for details see Table I of Ref. [72]).

The isobaric molar heat capacity $c_p(T)$ of the samples was determined in different calorimeters as described in Sec. I of Ref. [72]. Depending on the mass of the crystals and the type of the calorimeter, one or few well-formed specimens were selected for the measurements. Thermodynamic standard values (enthalpy and entropy at 298.15 K) are important for modeling of chemical transport reactions. Thus they may be useful for an optimization of the synthesis of boracite crystals. For the calculation of these values (Table II of Ref. [72]), data from all calorimetric measurements were combined.

The magnetization was measured in a SQUID magnetometer (MPMS-XL7, Quantum Design) from 1.8 to 400 K. A few smaller crystals were oriented randomly in the sample holder. Magnetization was recorded both in field-cooling (fc) and in warming after zero-field cooling (zfc). The magnetic fields H are nominal values [127].

III. CRYSTAL STRUCTURE OF BORACITES

Due to the formation of FE/FEla domains the full crystal structure of many boracites at low temperatures remains unknown up to now. However, for a first interpretation of the magnetic ordering phenomena, the knowledge of the point groups of the structure is sufficient. As an example of the basic structural motif of a cubic and of an orthorhombic boracite

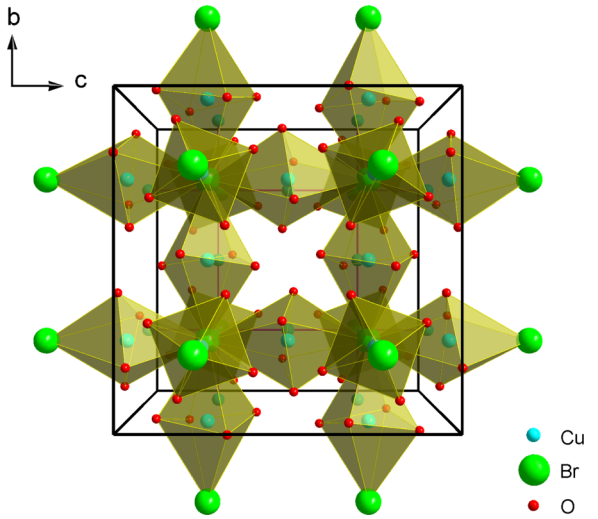

FIG. 1. (Color online) Simplified representation of the crystal structure of a cubic boracite ($Cu_3B_7O_{13}Br$, space group $F\bar{4}3c$) [128]. Boron and some oxygen atoms are omitted for clarity. Chains of elongated CuO_4Br_2 units (yellow) run along the linear Cu–Br chains in all three cubic space directions.

structure simplified representations of the Cu-Br [128] and of the Ni-Cl boracite [129] structure are given in Figs. 1 and 2. The transition-metal ions are surrounded by four close oxygen ions (M−O distance typically 200 pm). These MO_4 plaquettes deviate significantly from planarity (see, e.g., Ref. [130]) in both the cubic and noncubic phases. The MO_4 unit and especially the B-O network in boracites are relatively rigid [130] and the lattice parameters are therefore determined by the weaker metal-halogen bonds and thus by the ionic radii of the M and—to a lesser extent—of the X species. This is demonstrated in Fig. 3, where the (quasi)cubic lattice parameter a of the boracites is plotted against the ionic radii (IR) of the M^{2+} cations. a is linearly dependent on the IR of

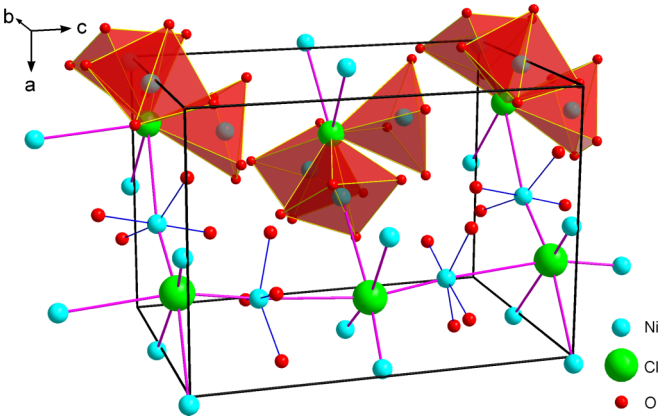

FIG. 2. (Color online) Simplified representation of the crystal structure of an orthorhombic boracite ($Ni_3B_7O_{13}Cl$, space group $Pca21$) [129]. Boron atoms and some oxygen atoms are omitted for clarity. Non-planar NiO_4 plaquettes are oriented perpendicular to corrugated chains (magenta) with short-long-short-long Ni–Cl bonds. Three NiO_4 plaquettes share a common Cl atom (red polyhedra) through short Ni–Cl bonds.

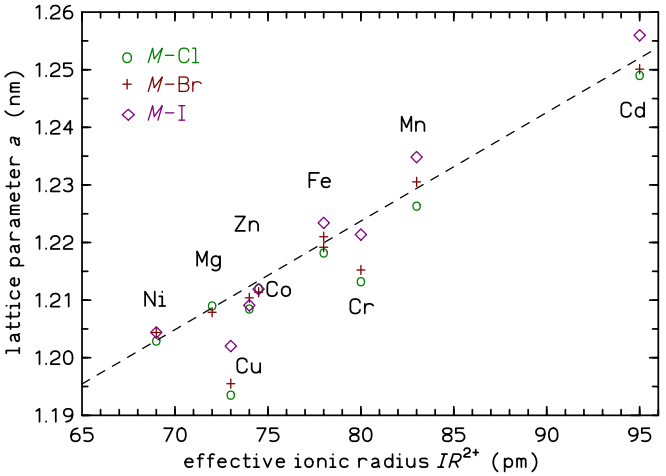

FIG. 3. (Color online) Cubic or quasicubic lattice parameter a at room temperature of the M-X boracites (M-Cl: o; M-Br: +; M-I: ◇) plotted against the effective ionic radii of the M^{2+} ions (coordination VI, high-spin state) [134]. The dashed line is a linear fit to the data where Cu-X and Cr-X boracites were excluded (see text). References: Mg-Cl [135]; Mg-Br [136]; Mg-I (no value known); Cr-Cl [137]; Cr-Br [130]; Cr-I [138]; Mn-Cl [139]; Mn-Br [140]; Mn-I [131]; Fe-Cl [141]; Fe-Br [142,143]; Fe-I [144]; Co-Cl, Co-I [99]; Co-Br [129]; Ni-Cl [129]; Ni-Br [145]; Ni-I [146]; Cu-Cl [99]; Cu-Br [128]; Cu-I [147]; Zn-Cl [142]; Zn-Br, Zn-I [99]; Cd-Cl [148]; Cd-Br, Cd-I [99].

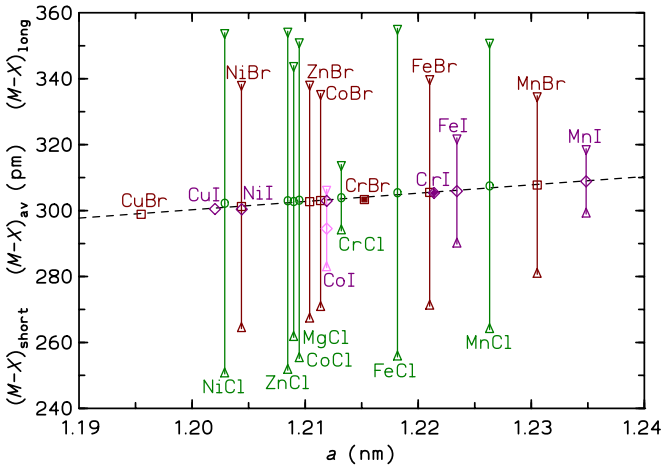

FIG. 4. (Color online) M-X bond distances of the M-X boracites plotted against the cubic or quasicubic lattice parameter a, mostly at room temperature. Averaged short and averaged long M-X distances are marked by up and downward pointing triangles, respectively. The total average (av) of all M-X distances are marked by different symbols/colors (M-Cl: ○/green; M-Br: □/red; M-I: ◇/magenta). The dashed line is a linear fit to the total average distances. The values for Co-I at $T = 31$ K (Ref. [149]) lie clearly below the trend and were excluded from the fit. Full symbols indicate compounds that stay cubic below the magnetic ordering temperature (down to 2 K). References for M-X distances: Mg-Cl [15]; Cr-Cl ($T = 100$ K) [132]; Cr-Br [130]; Cr-I [138]; Mn-Cl [139]; Mn-Br [140]; Mn-I [131]; Fe-Cl [141]; Fe-Br [143]; Fe-I [150]; Co-Cl [133]; Co-Br [129]; Co-I ($F\bar{4}3c1'$) [128]; Ni-Cl [129]; Ni-Br [151]; Ni-I [152]; Cu-Cl, no data known; Cu-Br ($F\bar{4}3c1'$) [128]; Cu-I [147]; Zn-Cl [94]; Zn-Br [153].

the M^{2+} ion, except for the Jahn-Teller ions Cr^{2+} and Cu^{2+}. The lattice parameter a increases with the halogen X in the order Cl, Br, I. For the 3d-metal boracites, a varies between 1.1935 nm for Cu-Cl [99] and 1.2349 nm for Mn-I [131], i.e., only by about 3.5%.

Along the a, b, and c axes the MO_4 plaquettes are aligned on M-X chains. In the cubic phase these chains are linear with equal M-X distances and the two different orientations of the MO_4 plaquettes alternate. Together with the X ions the plaquettes form a three-dimensional network of MO_4X_2 units (Fig. 1). The magnetic M^{2+} species occupy only one Wyckoff site 24c. In the orthorhombic phases three 4a sites are occupied by the M cations and the bonding distances follow a X-M—X-M—X short-long-short-long sequence. Figure 4 displays the averaged short, long, and the overall average M-X distances for the M-X boracites where the noncubic crystal structure is known. The differences between these averaged short and long M-X distances, $(\Delta[M\text{-}X])_{av}$, vary in the wide range from 20 pm (Mn-I [131], Cr-Cl) [132] to 103 pm (Zn-Cl [94], Ni-Cl) [129]. For the individual M-X boracite this difference gives an indication of the amount of distortion away from the cubic structure. For some boracites these distortions are so strong that the coordination environment of the M^{2+} ions degenerates to a distorted pyramid (4+1 coordination). This is illustrated for Ni-Cl boracite in Fig. 2, where the $M-$O bonds are on average 202 pm and the average short M-X bond is only 250 pm. For a given transition metal, the chlorine compound shows the largest distortion, viz. $(\Delta[M\text{-}X])_{av}$ and the iodine species the smallest or no detectable distortion (see Table I and Fig. 4).

Further crystal-structural observations have been discussed in Ref. [133], where correlations of the M-X distances with the difference in the Pauling electronegativity (EN) of the ions were pointed out. For increasing ΔEN the short M-X bond becomes shorter while the longer bond becomes longer. With increasing ΔEN also the sum of the long and short M-X bonds becomes larger.

Moreover, in $Ni_3B_7O_{13}Cl$, for the chains running in the ab plane the coordinations of Ni(2) and Ni(3) are rather similar while the chain running in c direction with the Ni(1) ion is different [129]. Two distinct M sites are also observed for Co-Br [129] and other orthorhombic boracites.

There are no detailed investigations on magnetic exchange in boracite structures up to now. As can be taken from Table I, only few boracites remain structurally cubic at low temperatures, notably the Cr-Br and Cr-I compounds. In these phases the M-X distances along the chains are all the same and the chains cross under 90°. With dominant AFM super-exchange between the nearest-neighbor M^{2+} ions and sizable (possibly competing) next-nearest-neighbor exchange not all interactions can be satisfied in a simple magnetic structure. The arrangement of magnetic moments in cubic boracites is thus prone to geometric frustration. In distorted boracite structures, especially for large values of $(\Delta[M\text{-}X])_{av}$ (many chlorine boracites; cf. Fig. 4), the M^{2+} ions are arranged in triangular pyramidal groups XM_3 with three short M-X bonds. These quite isolated triangular groups can be the origin of local frustration of the nearest-neighbor AFM interactions. The effect of further exchange interactions is difficult to determine and may even lead to low-dimensional behavior of

the whole spin system, which is not obvious from the simple description of the crystal structure.

Generally, any low-dimensional character or geometric frustration of magnetic exchange will lead to the appearance of short-range order and a suppression of the long-range ordering temperature. The ratio of the Weiss temperature (obtained from the paramagnetic susceptibility) and (Néel) ordering temperature, $|\theta_P|/T_N$, is a first indicator of such features in a spin system. For suitable arrangements of spins, sizable geometric frustration is said to be present when $|\theta_P|/T_N > 6$ [154–157]. None of the investigated cubic boracite compounds meets this benchmark. For strong geometrical frustration a spin-liquid state may form at low T. In such a case, long-range order is often facilitated by a symmetry-breaking structural PT at low T [154–158].

The various ways and degrees of distortion in boracite phases provide a vast playground for detailed future experimental and theoretical studies. Presumably, quite different kinds of geometrical frustration and low-dimensional magnetic exchange as well as orbital degrees of freedom lead to the observed complex magnetic ordering phenomena. The theoretical treatment of the magnetic exchange in boracites (e.g., by density-functional theory methods) is challenging due to the large unit cells and has to be deferred to further combined in-depth studies of the most-interesting boracite M-X species.

IV. ANALYSIS OF SPECIFIC HEAT DATA

At temperatures well below the structural PTs, the specific heat $c_p(T)$ of the "magnetic" boracites is

$$c_p(T) = c_{\rm lat}(T) + c_{\rm mag}(T), \qquad (1)$$

where $c_{\rm lat}$ is the lattice (phononic) heat capacity and $c_{\rm mag}$ is the contribution from the magnetic degrees of freedom of the M sublattice. The Zn^{2+} ion in Zn-X boracites has a nonmagnetic $3d^{10}$ configuration.

The molar mass of the Cr-Cl boracite is ≈8% lower than that of the Zn-Cl compound, and the differences in molar mass between the chlorine and bromine and iodine compounds are of the same amount or twice as large, respectively. The phonon modes related to the M and heavier X atoms are expected to lie at low frequencies while the stiff boron-oxygen network will vibrate at higher frequencies. This picture is confirmed by Raman and density-functional theory studies on the cubic phases of the Co-X boracites [97]. Clear peaks in the calculated phonon density of states are visible at 60–80 cm^{-1} for Co-I and at ≈80 cm^{-1} for Co-Br boracites [97].

The specific heat of the zinc boracites Zn-Cl, Zn-Br, and Zn-I, can serve as reference for the lattice contributions of the magnetic M-X species, respectively,

$$c_{\rm mag}(T)[M\text{-}X] \approx c_p(T)[M\text{-}X] - c_p(T)[\text{Zn-}X]. \qquad (2)$$

A good approximation can be expected for M-X boracites, which are isostructural to the respective Zn-X boracite and have similar lattice volumes, molar masses, and degree of distortion $(\Delta[M\text{-}X])_{\rm av}$ (cf. Fig. 4). Zn-Cl should be a good lattice reference for the isostructural rhombohedral Co-Cl and Fe-Cl. Zn-Br (orthorhombic) is isostructural with Cu-Br, Ni-Br, Co-Br, Mn-Br but not with Fe-Br (rhombohedral). Zn-I (orthorhombic) is isostructural with Co-I, Mn-I, and almost with Ni-I (weak monoclinic distortion), but not with Cu-I, Fe-I, and Cr-I. Since their lattice parameters differ strongly from the respective Zn compounds a less good approximation of $c_{\rm lat}(T)$ is expected for Cu and Mn boracites.

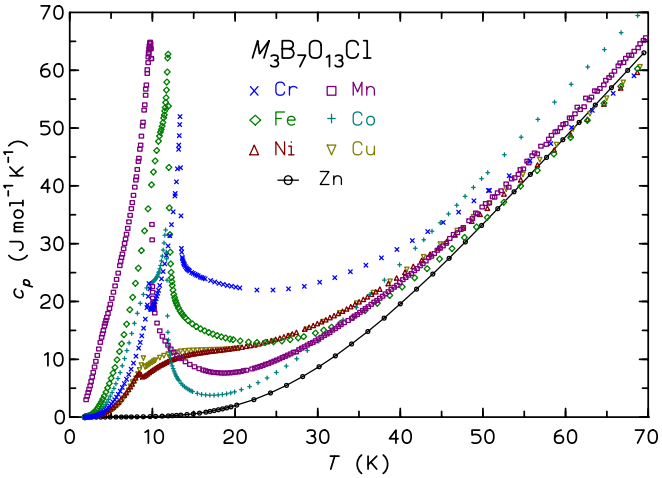

FIG. 5. (Color online) Molar heat capacity $c_p(T)$ of M-Cl boracites below 70 K. The curve of Zn-Cl can serve as reference for the lattice specific heat of the other M-Cl boracites.

In Fig. 5, the specific heats $c_p(T)$ of the chlorine boracites M-Cl are plotted. All curves (except for Co-Cl) join at 60–70 K, indicating that at this temperature the magnetic contribution to $c_p(T)$ becomes negligible and that the approximation for the lattice contribution by the specific heat of Zn-Cl boracite is justified. The evolution of the magnetic entropy $S_{\rm mag}$ with T gives information about the energy levels of the magnetic ions. It is obtained by integration of $c_{\rm mag}/T$. For temperatures below the first data point a T^3 extrapolation of $c_{\rm mag}$ is employed. The magnetic contributions for the bromine and iodine boracites are calculated the same way.

The transition temperatures T_t for all PTs investigated in our study are given in the structural sequences and can be compared with the values from previous investigations given in parentheses or in Ref. [72] Table III.

V. MAGNESIUM CHLORINE AND ZINC BORACITES

The specific heat of a powder sample of synthetic $Mg_3B_7O_{13}Cl$ (space group $Pca2_11'$) between 25 and 100 K is given in Fig. 6. As expected from the hardness of the crystals and from the light constituent atoms, $c_p(T)$ is very small at low T. The equivalent Debye temperature [159–161] $\Theta_D(T)$ varies between 660 and 790 K (see Ref. [72], Fig. 1 inset). For natural boracite from the Inder deposit, Kazakhstan (composition $Mg_{3.007}B_{6.995}O_{13}Cl$), $c_p(T)$ was determined between 14 and 321 K by Gurevich *et al.* [76]. Between 25 and 100 K their data agree with ours within 4% (see Fig. 6).

The low-temperature specific heat of Zn-Cl boracite (space group $R3c1'$) may be fitted by the first two terms of the harmonic lattice approximation [159–161], i.e., $c_p(T) = \beta T^3 + \delta T^5$ with $\beta = 9.86(7) \times 10^{-5}$ J mol^{-1}K^{-4} and $\delta = 3.5(1.3) \times 10^{-8}$ J mol^{-1}K^{-6}. The initial Debye temperature calculated from β is high [$\Theta_D(0) = 779$ K]. The specific heat of dielectric crystals can be analyzed by plotting the

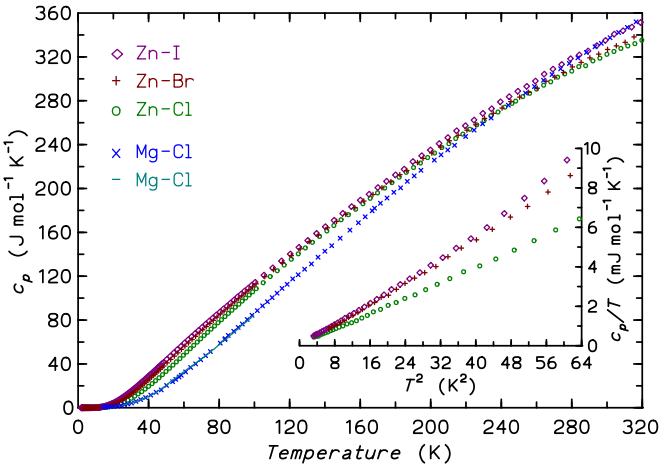

FIG. 6. (Color online) Molar heat capacity of Zn-Cl (o), Zn-Br (+), and Zn-I (◇) boracites measured in the PPMS calorimeter and of Mg-Cl boracite (×, data from [76]; continuous line, linking 126 data points, this work). The inset shows the Zn-X boracite data in a c_p/T vs T^2 representation.

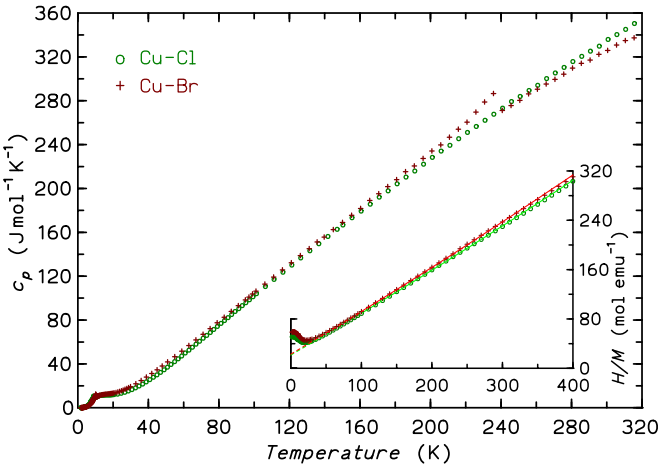

FIG. 7. (Color online) Molar heat capacity of Cu-Cl (o) and Cu-Br (+) boracites up to 320 K. The inset shows the inverse magnetic susceptibility $H/M(T)$ for $H = 10$ kOe and the modified Curie-Weiss fits (lines; see text).

equivalent Debye temperature curve $\Theta_D(T)$, which has a typical temperature dependence [159–161]. For $Zn_3B_7O_{13}Cl$ (Ref. [72], Fig. 1 inset), $\Theta_D(T)$ is constant [$=\Theta_D(0)$] for $T < 8$ K, then the curves gradually decreases towards a minimum which typically occurs at a temperature of $\Theta_D(0)/20$ [159,160]. Here, the minimum is observed at 32 K. Towards room temperature $\Theta_D(T)$ increases strongly [$\Theta_D(300\ \text{K}) \approx 1100$ K] due to the prevailing optical phonon modes of the light atoms.

For Zn-Br boracite (space group $Pca2_11'$) $c_p(T)$ is larger than that of Zn-Cl (Fig. 6). $c_p(T)$ already shows a significant positive deviation from the Debye T^3-law above 7 K. A fit results in $\beta = 1.242(7)\times10^{-4}$ J mol^{-1}K^{-4} and $\delta = 25.3(1.5)\times10^{-8}$ J mol^{-1}K^{-6} for the T^3 and T^5 terms, respectively. The characteristic Debye temperatures are lower (cf. Ref. [72], Fig. 1 inset): $\Theta_D(0) = 721$ K, $\Theta_{D,\text{min}}(T) = 465$ K at 28 K.

$c_p(T)$ of Zn-I boracite (space group $Pca2_11'$) shows no anomalies (Fig. 6) and the positive deviation from T^3 behavior becomes noticeable already at 6 K (Fig. 6 inset). A fit results in $\beta = 1.323(9)\times10^{-4}$ J mol^{-1}K^{-4} and $\delta = 1.7(3)\times10^{-7}$ J mol^{-1}K^{-6}. The Debye temperatures are lower than for Zn-Br: $\Theta_D(0) = 706$ K, $\Theta_{D,\text{min}}(T) = 427$ K is observed at 24.5 K. $c_p(300\ \text{K})$ for Zn-I is larger by ≈3% than for Zn-Cl and Zn-Br, obviously due to precursor effects of the structural PT at 366.4 K.

VI. COPPER BORACITES

Among the copper boracites, measurements could be performed on excellent large Cu-Cl and Cu-Br multidomain crystals. Cu-I is cubic at room temperature and can be obtained by high-pressure synthesis [120,147], but was not available in sufficient purity and quantity. For Cu-I, a higher magnetic ordering temperature than for Cu-Cl and Cu-Br can be expected.

A. $Cu_3B_7O_{13}Cl$

Cu-Cl boracite has the phase sequence

$$F\bar{4}3c1'(\bar{4}3m1') \leftarrow (369\ \text{K})\ [84]\ 369.4(1.0)\ \text{K} \rightarrow Pca2_11'(mm21') \leftarrow 8.9(2)\ \text{K}$$
$$(mm2?) \leftarrow (8.4\ \text{K})\ [118]\ (8.5\ \text{K})\ [119]\ 7.6(2)\ \text{K} \rightarrow Pc'a'2_1(m'm'2).$$

The symmetry of the weakly FM orthorhombic phase $m'm'2$, where both spontaneous magnetization and spontaneous polarization are aligned along the binary axis, has been deduced from measurements of the magnetic torque [118] and the ME effect [119]. The reported Néel temperatures T_N are 8.4 and 8.5 K, respectively.

At first sight, these temperatures agree well with the present $c_p(T)$ data (Figs. 7 and 9) which show a small peak at $T_{N1} = 8.9$ K. Magnetic susceptibility M/H in various fields is displayed in Fig. 8. A spontaneous magnetization is seen which increases in the usual way with decreasing T. The value extrapolated to $T = 0$ for our polydomain crystal is 0.003 μ_B/f.u. (at $H = 40$ Oe), which is lower than for a single ferroelectric domain (0.0071 μ_B/f.u. [118]). Surprisingly, this weak FM moment appears only below a temperature of 7.5–8.0 K. Indeed, in $c_p(T)$, a tiny second peak marks this transition at $T_{N2} = 7.6$ K. Thus we have to assign this small transition peak to the appearance of the $m'm'2$ phase. In M/H a cusp is visible for various fields at T_{N1} (Fig. 8 inset) indicating the presence of a purely AFM phase between T_{N1} and T_{N2}. Presumably, this phase is the $mm2$ phase, in analogy to Cr-Cl.

In the magnetic specific heat $c_{\text{mag}}(T)$, the ordering peak at T_{N1} sits on the rising slope of a broad anomaly with a maximum of 11.2 J mol^{-1}K^{-1} at 14.0 K. The magnetic entropy $S_{\text{mag}}(T)$ reaches $R\ln 2$, as expected for the $S = 1/2$ ion Cu^{2+}, but only 17% of this limiting value are released at T_{N1}. $\chi(T)$ shows a broad hump around 20 K, as typical for low-dimensional quantum magnets and/or frustrated spin systems. Curie-Weiss fits to $\chi(T)$ (corrected for the sum χ_{dia} of the diamagnetic increments [162], see Fig. 7 inset)

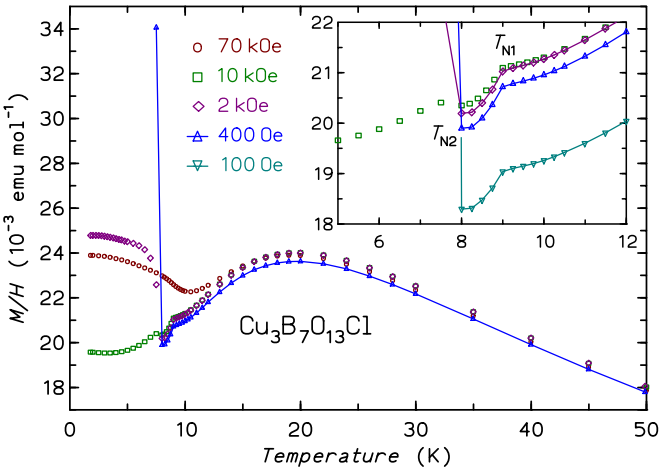

FIG. 8. (Color online) Magnetic susceptibility M/H of three randomly oriented crystal pieces of Cu-Cl boracite in different fields. The weak FM signal for 400 Oe rises to values out of the frame. The inset shows a magnification around $T_{N1/2}$.

at high temperatures (100–400 K) yield an effective moment of 3.48 μ_B/f.u. (2.01 μ_B/Cu atom, resulting in a g factor of 2.32, indicating large spin-orbit coupling [163]) and $\theta_P = -32.3(3)$ K, in fair agreement with previous data [164]. The ratio of Weiss and Néel temperature, $|\theta_P|/T_N$, is 3.6 for Cu-Cl. The magnetic exchange in Cu-Cl is presumably similar as in Ni-Cl which shows the same phenomena (discussion in Sec. VII A).

At temperatures below T_{N2}, $c_{\rm mag}(T)$ is $\propto T^3$, which is a signature of AFM magnon excitations. Below 4 K, a decrease of $c_{\rm mag}$ with increasing field is seen [165]. This might be connected to the observation, that at 4 K and for $H \geqslant 8$ kOe–depending on the direction – a magnetic field-induced PT had been detected by means of the ME effect [119]. The PT at T_{N2} has vanished in $c_p(T)$ for $H = 30$ kOe, but is still visible in $\chi(T)$ in 10 kOe. It can be assumed that the AFM ($mm2$) phase exists only for $H < 30$ kOe. In order to establish a magnetic phase diagram measurements on single domains are necessary.

B. $Cu_3B_7O_{13}Br$

Cu-Br boracite was known to transform like Cu-Cl from the cubic to the paramagnetic FE/FEla orthorhombic phase. In Cu-Br the small specific heat peak, observed in the present study at $T_{N1} = 10.0$ K, is also followed by a second, even smaller one at $T_{N2} = 8.9$ K (Fig. 9). M/H data are given in Fig. 10. The spontaneous magnetization appears between 8.8 and 9.0 K (i.e., at T_{N2}) and its value extrapolated for $T = 0$ is 0.0026 μ_B/f.u., similar to our Cu-Cl polydomain crystal. A weak cusp at T_{N1} marks the PT to a purely AFM phase. Thus, the proposed onset of the $m'm'2$ phase [120] occurs in fact at T_{N2}, being preceded in a small temperature interval by an AFM $mm2$ phase, analogous to Cr-Cl [42] and Cu-Cl. The total sequence of phases is

$$F\bar{4}3c1'(mm21') \leftarrow (243\ \text{K})\ [84]\ 230.5 \text{ and } 238.5\ \text{K} \rightarrow$$
$$Pca2_11'(mm21') \leftarrow (10\ \text{K})\ [120]\ 10.0(2)\ \text{K} \rightarrow$$
$$(mm2?) \leftarrow 8.9(2)\ \text{K} \rightarrow$$
$$Pc'a'2_1?(m'm'2?).$$

The magnetic susceptibility $\chi(T)$ at high T (Fig. 7 inset) is similar to that of Cu-Cl. The effective moment (range of fit 100–400 K, $\chi_{\rm dia}$ corrected) is 3.44 μ_B/f.u. (1.99 μ_B/Cu atom, thus $g = 2.30$) and $\theta_P = -33.7(3)$ K, in fair agreement with [164,166]. The magnetic specific heat above T_{N1} likewise indicates a low-dimensional character or frustration as discussed for Cu-Cl and Ni-Cl (see Sec. VII A). The entropy $S_{\rm mag}(T)$ at T_N is less than 20% of $R \ln 2$. Also for Cu-Br a field dependence of $c_{\rm mag}(T)$ is observed below ≈4 K. The magnetic phase diagrams and the exchange interactions of Cu-Cl and Cu-Br appear to be similar.

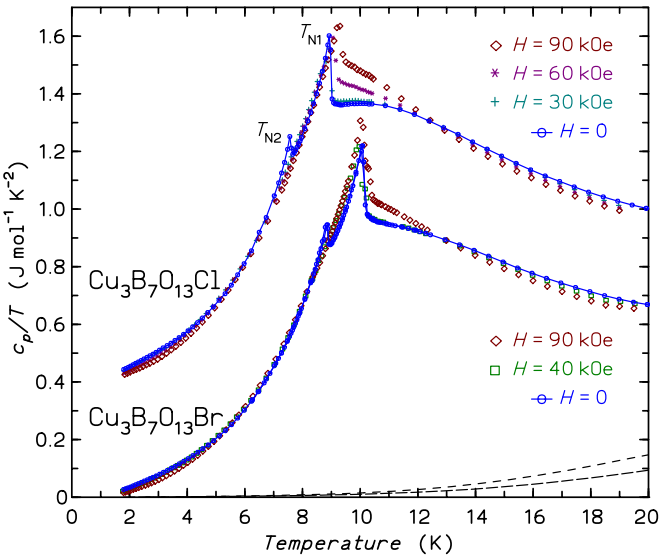

FIG. 9. (Color online) Molar heat capacity $c_p(T)/T$ of Cu-Cl (shifted up by 0.4 units) and Cu-Br boracites in different magnetic fields. The long (short) dashed line gives the estimated lattice heat capacity $c_{\rm lat}$ for Cu-Cl (Cu-Br) boracite.

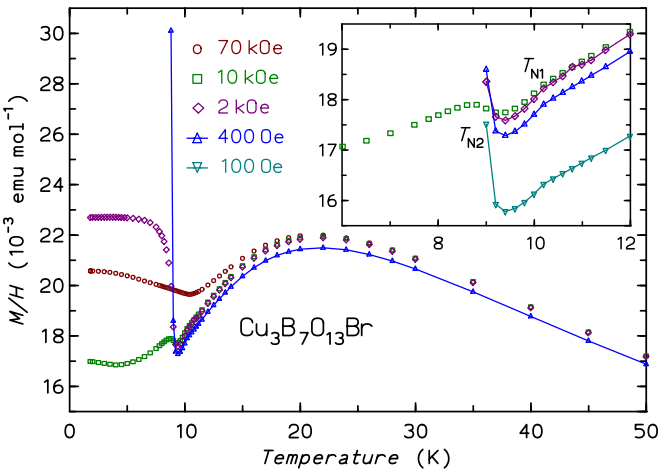

FIG. 10. (Color online) Magnetic susceptibility M/H of six randomly oriented crystal pieces of Cu-Br boracite in different fields. The weak FM signal for 400 Oe rises to values out of the frame. The inset shows a magnification around $T_{N1/2}$.

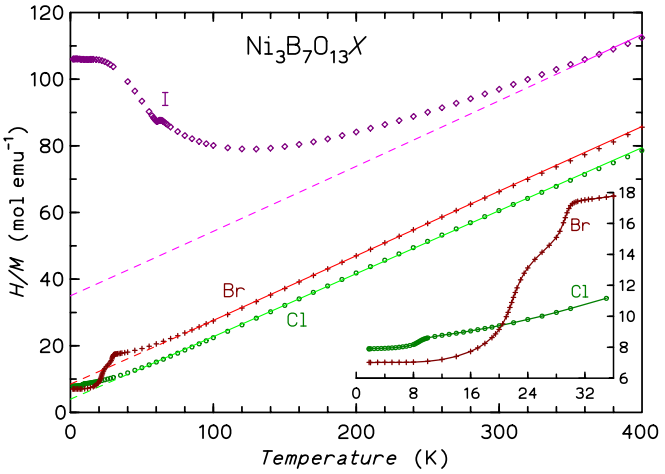

FIG. 11. (Color online) Inverse magnetic susceptibility of Ni-Cl, Ni-Br, and Ni-I boracites for $H = 10$ kOe. The lines are modified Curie-Weiss fits with diamagnetic corrections $\chi_{\rm dia}$ applied [162]. The inset shows a magnification.

VII. NICKEL BORACITES

The inverse magnetic susceptibility of the Ni boracites is given in Fig. 11. At high temperatures $\chi(T)$ of Ni-Cl and Ni-Br can be described by the Curie-Weiss law. The resulting effective magnetic moments and Weiss temperatures are: Ni-Cl, range of fit 50–400 K, $\mu_{\rm eff}$/Ni atom $= 3.79\ \mu_B$, $\theta_P = -21.4(4)$ K. Ni-Br, range 80–400 K, $\mu_{\rm eff}$/Ni atom $= 3.75\ \mu_B$, $\theta_P = -44.8(3)$ K. For Ni-I, a strong curvature of $1/\chi(T)$ is observed. In order to estimate θ_P we fitted $\chi(T)$ in the range 350–400 K and fixed $\mu_{\rm eff}$ to the value determined for Ni-Br. We obtain $\theta_P = -214$ K as a maximum (negative) estimate.

The $\mu_{\rm eff}$ of Ni-Cl and Ni-Br are in agreement with those deduced for low T by Quezel *et al.* [164], but for Ni-Br larger than the value 3.4(1) μ_B/Ni atom given by Mao *et al.* [167]. The $\mu_{\rm eff}$ values for all three compounds are well above the spin-only value 2.83 μ_B for a $S = 2$ ion, resulting in large g factors of 2.68 and 2.65, respectively. This may be due to spin-orbit coupling, which can result in values $\mu_{\rm eff} \leqslant g_J[J(J+1)]^{1/2} = 5.59\mu_B$ for Ni^{2+} with $L = 3$. The spin-orbit coupling parameter ζ of Ni d^8 is large allowing strong orbital effects. The origin of the unusual orbital contributions to $\mu_{\rm eff}$ is probably the characteristic 4+1 coordination of Ni^{2+} in Ni-Cl and Ni-Br. Especially, for Ni-Cl the short and long M-X distances have the largest average difference among the investigated boracites (cf. Fig. 4). The negative θ_P values indicate predominant AFM exchange interactions, increasing in the sequence Cl-Br-I with extraordinary strong AFM interactions for Ni-I.

A. $Ni_3B_7O_{13}Cl$

The phase sequence of Ni-Cl boracite is analogous to that of Co-Br, Co-I, Mn-Cl, Mn-Br, and Mn-I:

$$F\bar{4}3c1'(\bar{4}3m1') \leftarrow (608\ \text{K})\ [84]\ 591.3{-}606.7(1.0)\,\text{K} \rightarrow$$
$$Pca2_11'(mm21') \leftarrow (9\ \text{K})\ [115,116]\ 8.6(1)\text{K} \rightarrow$$
$$Pc'a2_1'(m'm2').$$

Long-range magnetic order in Ni-Cl sets in at $T_N = 8.53(5)$ K, as can be seen from the appearance of a weak

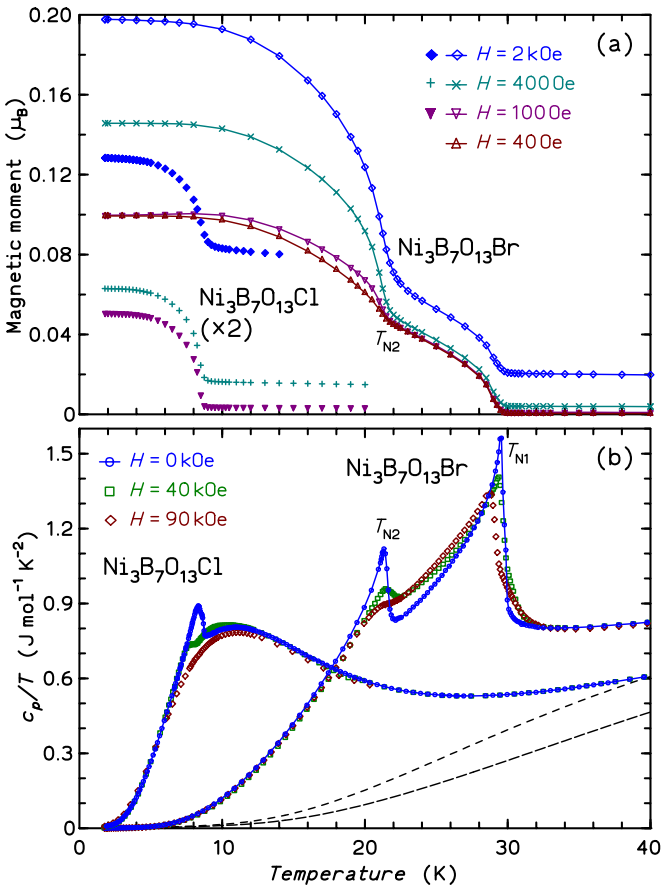

FIG. 12. (Color online) (a) Magnetization $M(T)$/f.u. of Ni-Cl (full symbols) and Ni-Br boracite (open symbols with line) for different magnetic fields. (b) Molar heat capacity c_p/T of Ni-Cl and Ni-Br boracites in different magnetic fields. The long (short) dashed line shows the lattice heat capacity of the Zn-Cl (Zn-Br) boracite using $f = 0.95$ (see text).

spontaneous magnetic moment [$M_s = 0.023\ \mu_B$/f.u. extrapolated to $T = 0$, Fig. 12(a)]. The T_N is consistent with previous torque magnetometry measurements ($T_N = 9.7$ K) [115]. Moreover, $T_N \approx 9$ K was determined from measurements of the ME effect [116,168], and from the integrated intensity of a magnetic neutron reflection [169]. The magnetic moment for our nonoriented polycrystalline sample is (as expected) smaller than for a single-domain sample (0.064 μ_B/f.u. [115]).

The specific heat anomaly at T_N is manifested as a small peak at 8.6 K [Figs. 13 and 12(b)]. A particular feature of Ni-Cl is the magnetic contribution due to short-range order extending smoothly far above T_N. The broad maximum in $c_{\rm mag}(T)$ of 10.3 J mol^{-1}K^{-1} is observed at 16.1 K [in the plot c_p/T versus T this leads to a maximum at ≈12 K, cf. Fig. 12(b)]. The ratio $|\theta_P|/T_N$ of 2.51 is small. A frustration of the magnetic interactions in Ni-Cl—and presumably also in Cu-Cl and Cu-Br—was suggested to be due to short-range spin ordering with dominant AFM interaction along the 180° $Ni^{2+} - Cl - Ni^{2+}$ exchange pathways, but frustrated due to the 90° $Ni^{2+} - Cl - Ni^{2+}$ pathways with competing FM interaction [169]. A second source of frustration may be the triangular pyramidal groups of $ClNi_3$ with three short Ni–Cl bonds, which is found analogously in all noncubic boracite

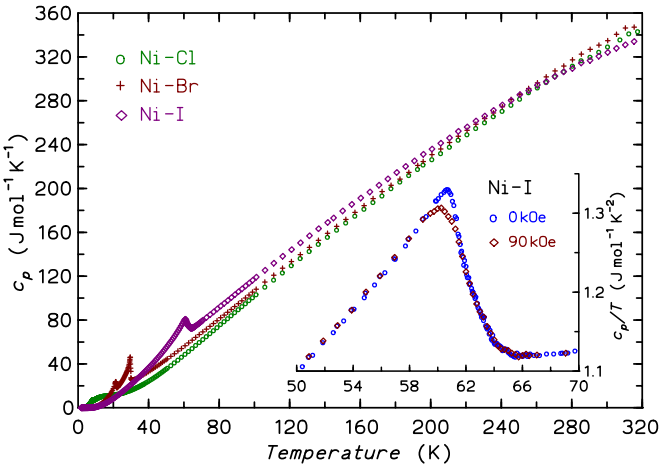

FIG. 13. (Color online) Molar heat capacity of Ni-Cl, Ni-Br, and Ni-I boracites. The inset shows a magnification of the transition peak of Ni-I for $H = 0$ and 90 kOe in a c_p/T representation.

structures [169], but which is particulary compact and isolated in Ni-Cl (and Cu-Cl) boracite due to the strong difference between short and long Ni–Cl bonds (cf. Figs. 2 and 4). The three-dimensional long-range ordering is marked by the small peak in $c_{\rm mag}$ at T_N. As for Cu-Cl, well below T_N a behavior close to $c_{\rm mag} \propto T^3$ is observed.

Surprisingly, the calculation of $c_{\rm mag}(T)$ by Eq. (1) yields negative values in the temperature range 57–250 K, suggesting severe differences in the lattice specific heat of Zn-Cl and Ni-Cl. This comes unexpected, since the lattice volumes of the Ni-X boracites are well in the trend observed for the M-X boracites (see Fig. 3). Since the same crossing of the $c_p(T)$ curves exists for Zn-Br and Ni-Br we assign this to a genuine difference and not to measurement inaccuracies. In order to get a positive $c_{\rm mag}(T)$ we used the modified formula $c_{\rm mag} = c_{{\rm Ni}X} - f \times c_{{\rm Zn}X}$ with $f = 0.95$. The obtained $c_{\rm lat}$ is shown as dashed line in Figs. 13 and 12(b). Irrespective of this correction, the resulting magnetic entropy of Ni-Cl (see Fig. 14) at T_N is only

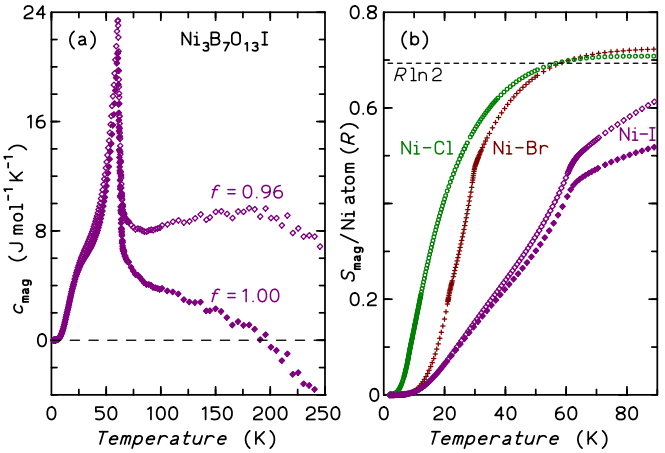

FIG. 14. (Color online) (a) Magnetic specific heat of Ni-I boracite. The alternative curves for $f = 1.00$ and 0.96 are show (see text). (b) Magnetic entropy $S_{\rm mag}(T)$ per Ni atom for Ni-Cl, Ni-Br, and Ni-I boracites. For Ni-I the two alternative curves are shown. The dashed line shows the entropy of $R \ln 2$ per Ni atom.

0.10 R per Ni atom, i.e., less than 15% of $R \ln 2$. $c_{\rm mag}(T)$ of Ni-Cl is qualitatively very similar to that of Cu-Cl and Cu-Br (cf. Fig. 9) in that the majority of the magnetic entropy is due to short-range interactions. Remarkably, for Ni-Cl the entropy $S_{\rm mag}$ at 100 K is only 0.71 $R \approx R \ln 2$ per Ni atom.

The zero field splitting (D) of the Ni^{2+} in the $^3A_2$ state in the axially distorted environment will lead to a singlet and a doublet state. Obviously, then the doublet should be the groundstate in Ni-Cl (effective spin 1/2) with a singlet state at higher energy $E = 2|D|$ ($D < 0$). However, in order to reproduce the experimental magnetic entropy $S_{\rm mag}(T)$ for Ni-Cl the splitting would be extremely large (see, e.g., Refs. [163,170]) and is thus unlikely to explain the magnetic specific heat of Ni-Cl.

Since the entropy is averaged over the three different Ni atoms of the Ni-Cl boracite structure [129] and $R \ln 2 \approx \frac{2}{3} R \ln 3$ one may speculate that only two of the three Ni^{2+} ions order magnetically. In a neutron diffraction study on a powder sample of Ni-Cl [169], the magnetic structure below T_N was determined at 1.5 K and refined in magnetic space group $Pc'a2'_1$. In this structure all three nonequivalent Ni^{2+} sites are bearing ordered moments, however, the moment of the Ni(2) and Ni(3) are only 0.79 μ_B, while for Ni(1) 1.65 μ_B are found. Thus two sites show a magnetic moment well below the expected value of $\approx gS$. These observations are in line with the low value of the magnetic entropy at T_N. The ratio of magnetic diffuse and Bragg scattering observed in Ref. [169] seems, however, not that large as expected for such a ground state. An inelastic neutron diffraction investigation could help to clarify this issue.

B. $Ni_3B_7O_{13}Br$

Ni-Br boracite undergoes the same phase transformations as Ni-Cl, but the orthorhombic FE/FEla/FM phase $Pc'a2'_1$ undergoes a further second-order magnetic PT to the lowest possible triclinic symmetry (point group 1):

$$F\bar{4}3c1'(\bar{4}3m1') \leftarrow (398\ {\rm K})\ [84]\ 394.8(1.0)\ {\rm K} \rightarrow$$
$$Pca2_11'(mm21') \leftarrow (29\ {\rm K})\ [117]\ 29.5(2)\ {\rm K} \rightarrow$$
$$Pc'a2'_1(m'm2') \leftarrow (21\ {\rm K})\ [117]\ 21.4(2)\ {\rm K} \rightarrow 1.$$

Detailed magnetization data on a FE/FEla/FM single domain crystal showed that the orientation of the spontaneous magnetization assumes a general crystallographic direction at 5 K [167]. The present data on a polydomain sample [Fig. 12(a)] are consistent with these data ($M_{\rm s,av} = 0.0025\ \mu_B$/f.u.). The two magnetic PTs are marked by sharp peaks in the specific heat at $T_{N1} = 21.4$ K and $T_{N2} = 29.5$ K, respectively [Fig. 12(b)], in agreement with the temperatures derived from measurements of spontaneous birefringence [117]. The triclinic phase, originally not recognized as such [171,172], was confirmed by ME and magnetooptical measurements [117], FM domain and domain wall studies [173], and by magnetization data [167]. Only an average orthorhombic magnetic structure determination by neutron diffraction on a powder sample was so far possible in the triclinic phase [151]. While the magnetization study [167] showed clear changes of the weak FM moment vector, no

change of the underlying AFM structure could be resolved at T_{N2} by neutron diffraction [151].

In contrast to the specific heat of Ni-Cl, the magnetic ordering peaks in Ni-Br are more of lambda-type, however, with a significant contribution of $c_{\rm mag}(T)$ above T_{N1} indicating the importance of short-range ordering in Ni-X boracites. Between 11 and 19 K $c_{\rm mag}(T)$ varies approximately $\propto T^3$. The magnetic entropy (Fig. 14) at T_{N1} is 69% of $R\ln 2$ per Ni atom (0.48 R), that at T_{N2} is less than half of this value (0.22 R). As for Ni-Cl, $S_{\rm mag}$ per Ni atom at 80 K is only 2/3 of the expected $R\ln 3 \approx R\ln 2$. In conjunction with the neutron diffraction results [151], which resulted in finite ordered moments for the Ni(2) and Ni(3) sites and zero ordered moment for Ni(1) (in Ni–Br chains along the orthorhombic c direction), the reduced entropy may be motivated. Therefore, for both Ni-Cl and Ni-Br, the question arises whether there exists a partially disordered phase. More detailed investigations on the magnetic structure and the spin fluctuations in Ni-Cl and Ni-Br are needed.

C. $Ni_3B_7O_{13}I$

Nickel iodine boracite is of particular interest because (1) it was the first material in which in the year 1966 the simultaneous occurrence of FE and (weak) FM in the same phase, i.e., a *multiferroic* state, was discovered [23], and (2) it is so far the only boracite in which these two properties, together with ferroelasticity, set on at the same temperature in a single PT from cubic to monoclinic symmetry:

$$F\bar{4}3c1'(\bar{4}3m1') \leftarrow (61.5\ \text{K})\ [45,106]\ 60.7-64.7\ \text{K} \rightarrow m'.$$

The monoclinic magnetic point group m' was established [45,106] on the basis of polarized light microscopic and ME studies, whereas initially [23] the orthorhombic symmetry $m'm2'$ was mimicked due to unrecognized layers of monoclinic domains, and the too low triclinic symmetry 1 was found by neutron diffraction [174] due to incompletely poled single crystals. The spontaneous magnetization is small; 0.0009 μ_B/f.u. for our polydomain crystal. The onset of the spontaneous magnetization (see Fig. 15) is broadened (61–64 K), even in fields as low as 20 Oe. The rounded maximum of $\chi(T)$ around 125 K (Fig. 15), together with the large $\theta_P = -214$ K in comparison to T_N, signal the severe frustration of the magnetic exchange interactions in the cubic phase (cf. Sec. XI).

The specific heat anomaly associated with this PT (Fig. 13) is characterized by a broad step with an extended falling flank between 60.7 and 64.7 K. In a measurement (not shown) using the DISC calorimeter on a set of five crystals a two-step structure on the falling flank could be observed, however, no latent heat was detected. This type of anomaly has to be compared with the sharp lambda-type peaks at the Néel points of most other boracites. We conclude that the PT in Ni-I is of *magnetostructural* type [105]. as discussed below in detail in the section on chromium boracites (Sec. XI). Here, the absence of detectable latent heat at the PT allows only for weak structural displacements, albeit they should be larger than in boracites showing lambda-type PTs. The structural coupling of the magnetic transition is corroborated by the observation

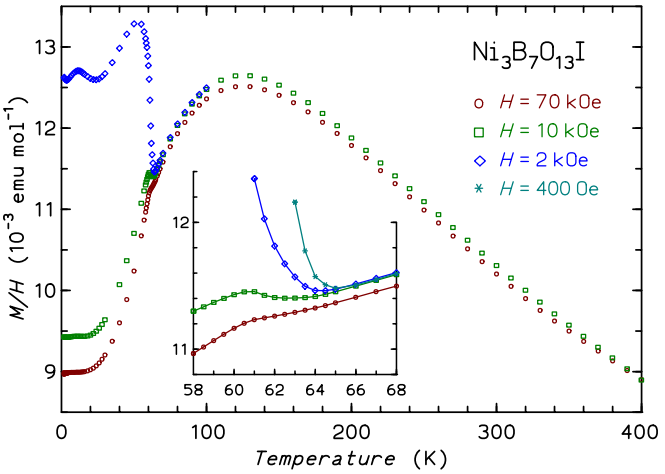

FIG. 15. (Color online) Magnetic susceptibility of Ni-I boracite in various magnetic fields. The inset shows a magnification around the PT temperature.

that T_N is very little influenced by a magnetic field of 90 kOe (Fig. 13 inset).

Moreover, the broadening of the PT is probably caused by differences in T_N for different growth sectors, as explained in the section IIJ of Ref. [72]. The euhedral Ni-I crystal measured on the PPMS calorimeter (Fig. 13) showed surface areas of 1/3 of 111 and 2/3 of $(\bar{1}\bar{1}\bar{1})$ facets. Using samples prepared from (100) growth sectors only, the measurement of the spontaneous polarization, permittivity, linear ME effect and piezoelectric effect [45,106,175] showed the PT to be sharp and of second order.

Due to the high T_N it is difficult to calculate the magnetic specific heat. The curves $c_{\rm mag}(T)$ in Fig. 14(a) were obtained as $c_{\rm NiI} - f \times c_{\rm ZnI}$ using $f = 1$ and $f = 0.96$, the latter yielding only positive $c_{\rm mag}$ below 310 K. $S_{\rm mag}(T_N)$ is between 0.45 R and 0.51 R per Ni atom (depending on the choice of f), which again is well below the expected entropy of $R\ln 3$ per Ni atom for a full three-dimensional long-range order of all Ni atoms. The PT peak sits on top of a broad magnetic contribution [see Fig. 14(a)] due to short-range correlation, which contributes significantly to the magnetic entropy above T_N. This is consistent with the high (absolute) Weiss temperature θ_P of Ni-I. In addition, a broad hump at around 35 K ($\approx T_N/2$) is visible, which may originate in a (continuous) spin reorientation. Such a reorientation may be linked with a symmetry allowed rotation of the spontaneous magnetization vector in the monoclinic m' plane.

VIII. COBALT BORACITES

The magnetic susceptibilities of the Co-X boracites (Fig. 16) at high T roughly follow the Curie-Weiss law, but those for Co-Cl and Co-Br are much better fitted when including a temperature-independent (paramagnetic) term $\chi_0 = \chi_{\rm dia} + \chi_{\rm TIP}$. The results of the fits above 80 K are: Co-Cl, $\chi_0 = +2.12(5) \times 10^{-3}$ emu mol^{-1}, $\mu_{\rm eff}$/Co atom = 5.01 μ_B, $\theta_P = -23.6(2)$ K; Co-Br, $\chi_0 = +0.91(8) \times 10^{-3}$ emu mol^{-1}, $\mu_{\rm eff}$/Co atom = 5.37 μ_B, $\theta_P = -31.7(3)$ K;

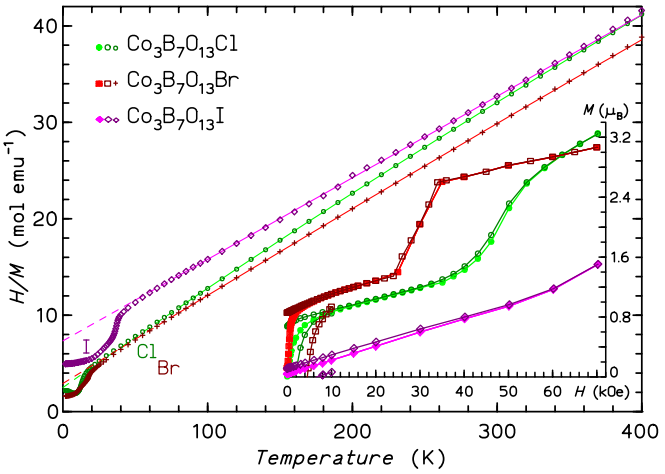

FIG. 16. (Color online) Inverse magnetic susceptibility of Co-Cl, Co-Br, and Co-I boracite for $H = 10$ kOe. The full lines are modified Curie-Weiss fits, the dashed lines show the extrapolations to $T = 0$. Inset: isothermal high-field magnetization curves $M(H)$ at 2.0 K. Curve parts with full symbols were taken with increasing field after zero-field cooling.

Co-I, fit excluding the structural PT region, $\mu_{\rm eff}$/Co atom = 5.62 μ_B, $\theta_P = -86.8(5)$ K.

As observed before [164,166], the $\mu_{\rm eff}$ per Co atom are all larger than 5.0 μ_B. Values for Co^{2+} (in octahedral environment 4.7–5.2 μ_B) are typically well above the spin-only value (3.87 μ_B) [163,170], while full $L-S$ coupling would result in 6.63 μ_B. The $\mu_{\rm eff}$ values for Co-Br and Co-I indicate extraordinarily strong orbital contributions, in line with our observations on Ni-X boracites.

The temperature dependence of the magnetization can be taken from Fig. 17 and the T_N are listed in Table III. The spontaneous FM moments M_s at 1.8 K are in fair agreement with those determined in Ref. [164] for 4.2 K (values in parentheses): Co-Cl 0.52 (0.78) μ_B/f.u.; Co-Br 0.84

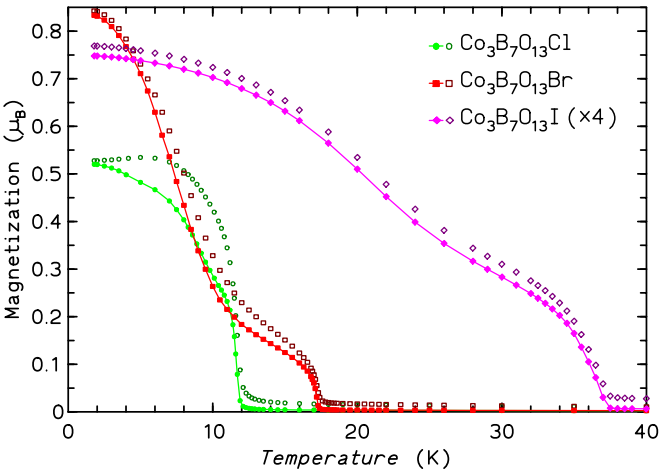

FIG. 17. (Color online) Selected low-field magnetization $M(T)$ data for Co-Cl, Co-Br, and Co-I boracites. Curves with open symbols were measured in field-cooling at $H = 400$ Oe, those with full symbols (connected by a line) in 100 Oe in heating after zero-field cooling. The data for Co-I are enlarged by a factor of 4.

(0.92) μ_B/f.u.; Co-I 0.19 (0.18) μ_B/f.u. M_s of Co-I is well below that of Co-Cl and Co-Br. Remarkably, $M_s(T)$ of all three Co compounds increases with decreasing T in two broad steps.

Isothermal $M(H)$ loops (inset of Fig. 16) at 2.0 K indicate the same sequence of the remanent magnetization M_r as observed for M_s (coercive field $H_{\rm cr}$ in parentheses): Co-Cl 0.67 (1.8), Co-Br 0.86 (4.6), Co-I 0.12 μ_B/f.u. (6.6 kOe). These values are different from those reported in Ref. [164], however, the present samples were magnetized in fields up to 70 kOe. For fields above the closing of the hysteresis, $M(H)$ increases linearly with H. Between 24 and 34 kOe Co-Cl shows a sharp transition to a spin configuration with higher magnetization (spin flop). In this spin state, $M(H)$ increases with almost the same slope as in the low-moment state. Similarly, $M(H)$ of Co-Cl displays a rounded step starting at ≈40 kOe and for Co-I a deviation from the linear behavior is seen above 60 kOe.

The specific heat of Co-X boracites is shown in Fig. 18 (data published earlier [125] showed large scatter). A characteristic feature of $c_{\rm mag}(T)$ of Co-X boracites are shoulder or hump-type ("Schottky-like" [125]) anomalies below T_N. These anomalies are also reflected in other physical properties, for which we compile data in Table III. Neutron diffraction has been performed on ^{11}B enriched polycrystalline samples of Co-Cl [180], Co-Br [181], and Co-I [149].

A. $Co_3B_7O_{13}Cl$

Co-Cl boracite shows the phase sequence

$$F\bar{4}3c1'(\bar{4}3m1') \leftarrow (\approx 623\ \text{K})\ [84,86]\ > 590(5)\ \text{K} \rightarrow$$
$$Pca2_11'(mm21') \leftarrow (\approx 538\ \text{K})\ [86]\ \rightarrow$$
$$m1' \leftarrow (\approx 468\ \text{K})\ [86]\ \rightarrow$$
$$R3c1'(3m1') \leftarrow (\approx 12\ \text{K})\ [86]\ 11.6\ \text{K} \rightarrow Cc(m),$$

which differs strongly from that of Co-Br and Co-I. The paramagnetic rhombohedral FE/FEla phase $R3c1'$ ($3m1'$), which has only one kind of cobalt site, undergoes a spin ordering to a monoclinic, fully FE/fully FEla and partially weakly FM phase of magnetic point group m [41,46,86]. Using neutron diffraction, the magnetic structure of that phase has been determined at 1.5 K and refined in the monoclinic space group Cc [180], in agreement with group-theoretical predictions [105].

Figure 19 shows the specific heat results. In zero magnetic field, a sharp transition (lambda-type at the high-temperature flank) is observed at 11.6 K, however, a broad shoulder is observed around 9.3 K. T_N as well as the temperature of the shoulder ($T_{\rm sh}$) lower with increasing H. For $H = 30$ kOe, we find $T_N = 11.4$ K and $T_{\rm sh} = 8.3$ K. For $H = 60$ kOe, transitions are observed at 10.0 K and at ≈2.1 K and for 90 kOe only one at 5.5 K. For $H = 30$ kOe, the peak, which can be assigned to T_N, appears broad, but the anomaly at 10.0 K for $H = 60$ kOe appears again sharper. For the latter field, the high-moment phase is seen in the $M(H)$ curve at 2.0 K.

The magnetoelectrically induced polarization P, measured at a dc magnetic field of 500 Oe, indicated $T_N \approx 12$ K and showed a sharp shoulder-type anomaly at about 11.3 K, connected with a change of slope of the coefficient $\alpha_{32}(T)$ of the linear ME effect [86]. Such a change in slope was also found at ≈10 K for the spontaneous Faraday rotation,

TABLE III. Néel temperatures T_N and temperatures (in K) of anomalies of various physical properties of Co-X boracites, possibly related to the shoulder or hump-type anomalies in the magnetic specific heat below T_N.

Boracite Co-X	Co-Cl	Co-Br	Co-I	references
T_N [peak in $c_p(T)$ / spont. moment]	11.6 / 11.9	17.1 / 17.3	36.5 / 37.0(5)	this work
$T_{sh/h}$ [shoulder or hump in $c_p(T)$]	≈10	≈8	≈22	[125]
spont. birefringence $\Delta n_s(T)$		≈10 (min. $\Delta n_{\gamma,\beta}$)	20 ± 2 (min. $\Delta n_{\gamma,\beta}$)	[176]
			≈28 (min. $\Delta n_{\gamma,\alpha}$)	[113]
ME-effect coefficient α_{ik}	11.4 (anomaly of α_{32})	≈10 (max. α_{32})	≈30 (min. α_{32})	[86,114,177]
spont. magnetization $M_s(T)$			≈29 (change of slope)	[178]
spont. Faraday rotation $\Theta_F(T)$	≈10 (change of slope)			[179]

whereas spontaneous polarization and dielectric permittivity were not sensitive to that anomaly [179]. From these data, it is not clear whether the shoulder-type anomaly is connected with a change in magnetic symmetry or not. Most probably the anomaly indicates a continuous spin reorientation in the ordered phase. Interestingly, the anomaly of magnetic field-induced polarization was absent at a field of 10 kOe, letting presume that the phase below 11.3 K can already be induced above 11.3 K by means of a magnetic field. Detailed studies will be required to elucidate the complex $T-H$ phase diagram.

The magnetic entropy $S_{mag}(T)$ (see Fig. 18) just above T_N is $R \ln 2$ per Co atom for Co-Cl (as well as for Co-Br and Co-I). Thus the ground state is a doublet (effective spin 1/2) at these low temperatures, as usually found for Co^{2+} with strong spin-orbit coupling [163,170,182,183]. At higher T, the spin 3/2 magnetism of the populated levels of the $^4T_1$ state is recovered (cf. the $R \ln 3$ level in Fig. 18). Judged from the development of $S_{mag}(T)$ and from the small $|\theta_P|/T_N$ the magnetic ordering in Co-Cl is essentially three-dimensional.

B. $Co_3B_7O_{13}Br$

The phase sequence of Co-Br is

$$F\bar{4}3c1'(\bar{4}3m1') \leftarrow (466\ \text{K})\ [84,113]\ 462.2(1.0)\ \text{K} \rightarrow$$
$$Pca2_11'(mm21') \leftarrow (17.5\ \text{K})\ [113]\ 17.1\ \text{K} \rightarrow$$
$$Pc'a2_1'(m'm2'),$$

which is analogous to that of Co-I, i.e., the cubic phase transforms to a paramagnetic, FE/FEla orthorhombic phase, which undergoes a PT to a weakly FM phase.

Neutron diffraction studies on $Co_3{}^{11}B_7O_{13}Br$ [181] revealed a two-step onset of magnetic ordering, starting at the second-order PT at $T_N = 17.5$ K and followed below about $T = 10.5$ K by a smooth transformation to a three-dimensionally canted magnetic structure of space group $Pc'a2_1'$. The transformation coincides with a minimum of magnetic birefringence $\Delta n_{\gamma,\beta}(T)$ at ≈10 K and with a maximum of the ME coefficient α_{32} at 10 K [177].

The zero-field specific heat of Co-Br (Fig. 20) shows a sharp lambda peak at $T_N = 17.1(1)$ K. A very pronounced hump is seen at $T_h = 8.0$ K and a corresponding minimum around 11.5 K. This anomaly obviously coincides with the above-described smooth magnetic transformation. The magnetic entropy (see Fig. 18) removed at 12 K is $1.9 \times R \ln 2$ if calculated per f.u. (3 Co atoms). The neutron diffraction data at 12 K and 1.5 K show structures with a three-dimensionally canted spin arrangement on the three cobalt sites, without involving a change in magnetic space group $Pc'a2_1'$. There is no paramagnetic Co sublattice below T_N as for Co-I (see below), i.e., all Co carry a sizable ordered moment.

With increasing magnetic field the humplike transition gradually decreases in size and shifts to lower T. As seen from the $M(H)$ isotherm at 2.0 K (Fig. 16 inset) the high-moment phase is entered around 60 kOe. We therefore assign

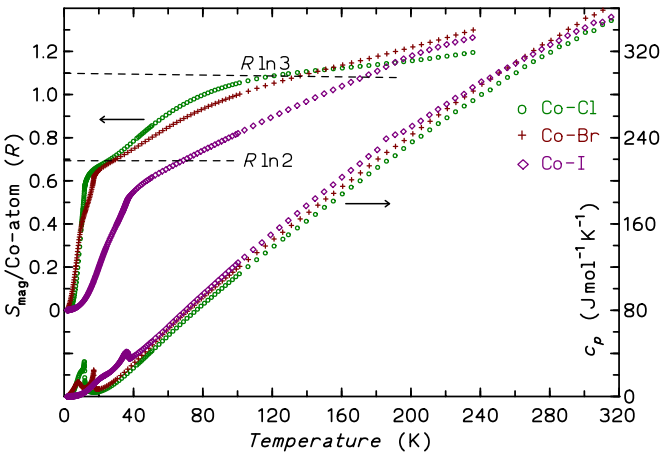

FIG. 18. (Color online) Molar heat capacity of Co-Cl, Co-Br, and Co-I boracite (right axis) and magnetic entropy $S_{mag}(T)$ per Co atom (left axis).

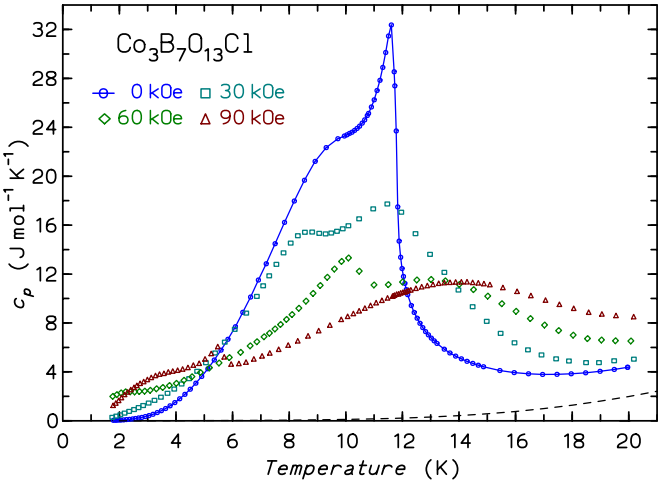

FIG. 19. (Color online) Molar heat capacity of Co-Cl boracite in various magnetic fields. The dashed line is the heat capacity c_{bg} of Zn-Cl boracite.

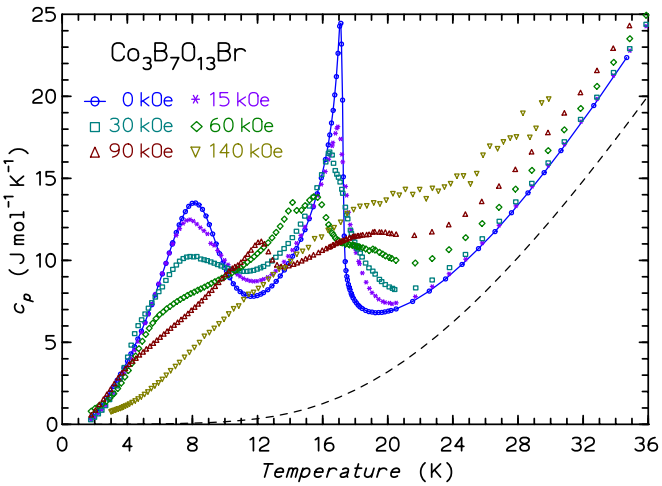

FIG. 20. (Color online) Molar heat capacity of Co-Br boracite in various magnetic fields. The dashed line is the heat capacity $c_{\rm bg}$ of Zn-Br boracite.

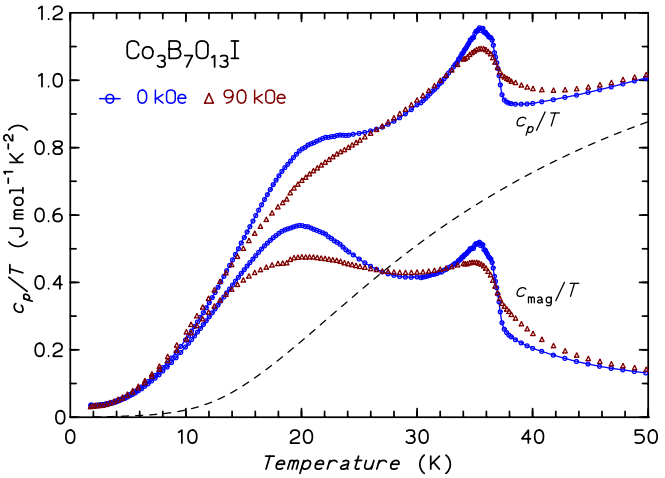

FIG. 21. (Color online) Molar heat capacity c_p/T of Co-I boracite in zero (○; connected by a line) and 90 kOe (△) magnetic field. The magnetic specific heat $c_{\rm mag}/T$ was obtained by subtracting the data of Zn-I boracite (dashed line).

the interval between T_h and T_N to the high-moment phase. Measurements on an oriented crystal are required to establish a phase diagram.

C. $Co_3B_7O_{13}I$

For Co-I boracite the sequence is analogous to Co-Br:

$$F\bar{4}3c1'(\bar{4}3m1') \leftarrow (\approx 194)\ \text{K}\ [84,114]\ \rightarrow$$
$$Pca2_11'(mm21') \leftarrow (37.5\ \text{K})\ [114]\ 36.5\ \text{K} \rightarrow$$
$$Pc'a2_1'(m'm2').$$

Neutron diffraction studies of the canted AFM structure of Co-I at 31 and 9 K have revealed a magnetic ordering in two steps, without any change in the magnetic symmetry of the weakly FM orthorhombic phase ($Pc'a2_1'$; $m'm2'$) [149]. Among the three crystallographically nonequivalent cobalt ions of the paramagnetic phase $Pca2_11'$, only the Co1 and Co2 sublattices are magnetically ordered at 31 K (Co1 3.43 μ_B, Co2 1.23 μ_B), whereas that of Co3 is ordered at 9 K also (Co1 4.19 μ_B, Co2 3.28 μ_B, Co3 1.8 μ_B) [149].

The magnetic specific heat for Co-I is shown in Fig. 21. This Néel transition is not a sharp lambda anomaly but two peaks are discernable at $T_{N1} = 36.4$ K and $T_{N2} = 35.4$ K, in spite of that the measurement was performed on one single crystal (measurements with heat-pulse calorimeters on several crystals resulted in the same splitting). One may speculate that the PT at T_{N2} is due to the ordering of the Co2 sublattice for which a low ordered moment was observed at 31 K [149].

A humplike anomaly with maximum at 20.0 K is observed in $c_{\rm mag}(T)$. Interestingly, a bend of $\Delta n_{\gamma,\beta}(T)$ at ≈20 K and a negative peak of the derivative $d\Delta n_{\gamma,\beta}/dT$ of the magnetic contribution to spontaneous birefringence [176] correspond to this hump. However, the change in slope of spontaneous magnetization $M_s(T)$ (cf. Fig. 16 inset), at ≈29 K and initially interpreted as a PT [178], coincides with a smooth minimum of the ME coefficient α_{32} at ≈30 K and the minimum of spontaneous birefringence $\Delta n_{\gamma,\alpha}$ at ≈28 K [113]. These temperatures merely coincide with the upper end of the hump in $c_{\rm mag}$. Both characteristic temperatures seem to be related with the stepwise ordering of the three Co sites. We speculate that the anomalies at ≈20 K are due to the buildup of magnetic moment on the Co3 site.

It was suggested by Jahn and Dachs [184] for AFM, optically uniaxial rutile-type fluorides that a one-to-one correspondence exists between the temperature derivative of the magnetic contribution to spontaneous birefringence and the magnetic heat capacity. In the case of the orthorhombic $m'm2'$ phases of boracites, the situation is more complicated, because of the three-dimensional spin arrangement and the three birefringence principal sections to be considered. A thorough theoretical treatment would be required in this case (compare, e.g., Ref. [185]), in order to correlate $c_p(T)$ and $d\Delta n/dT$ on the three orthorhombic principal sections.

IX. IRON BORACITES

The boracites Fe-Cl and Fe-I have the same sequence of phases as Co-Cl, i.e.,

Fe-Cl: $F\bar{4}3c1'(\bar{4}3m1') \leftarrow (609\ \text{K})\ [84]\ 611.2(1.0)\ \text{K} \rightarrow$
$Pca2_11'(mm21') \leftarrow (543\ \text{K})\ [84]\ 548.2(1.0)\ \text{K} \rightarrow$
$m1' \leftarrow (528\ \text{K})\ [84]\ 530.4(1.0)\ \text{K} \rightarrow$
$3m1' \leftarrow (11.5\ \text{K})\ [112]\ 11.85(10)\ \text{K} \rightarrow m,$

Fe-I: $F\bar{4}3c1'(\bar{4}3m1') \leftarrow (349\ \text{K})\ [84]\ 352.3(1.0)\ \text{K} \rightarrow$
$Pca2_11'(mm21') \leftarrow 200.9(1.0)\ \text{K} \rightarrow$
$m1' \leftarrow 183.0(1.0)\ \text{K} \rightarrow$
$3m1' \leftarrow (31\ \text{K})\ [112]\ 32.3(2)\ \text{K} \rightarrow m,$

but in Fe-Br the monoclinic phase $m1'$ is lacking:

$F\bar{4}3c1'(\bar{4}3m1') \leftarrow (495\ \text{K})\ [84]\ 500.6(1.0)\ \text{K} \rightarrow$
$Pca2_11'(mm21') \leftarrow (405\ \text{K})\ [84]\ 409.4(1.0)\ \text{K} \rightarrow$
$3m1' \leftarrow (18.5\ \text{K})\ [112]\ 18.25(20)\ \text{K} \rightarrow m.$

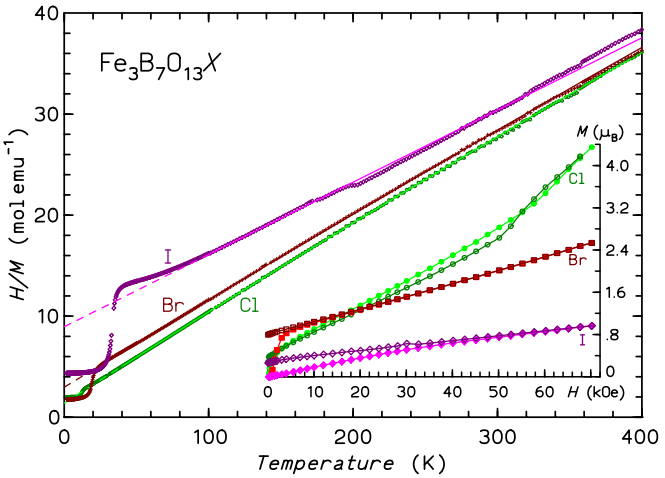

FIG. 22. (Color online) Inverse magnetic susceptibility of Fe-Cl, Fe-Br and Fe-I boracites in $H = 10$ kOe and modified Curie-Weiss fits (lines). Inset: magnetization curves at $T = 1.8$ K for increasing (full) and decreasing field (open symbols).

Whereas the magnetic point group m is well established for Fe-I by means of polarized-light optical-domain studies and domain-switching experiments [186,187] that symmetry is postulated as probable for Fe-Cl and Fe-Br.

The magnetic susceptibilities of the Fe-Cl and Fe-Br boracites (Fig. 22) at high temperatures are well described by the modified Curie-Weiss law including a T-independent term χ_0 (which is the sum of diamagnetism $\chi_{\rm dia}$ and a paramagnetic contribution $\chi_{\rm TIP}$). The resulting parameters are for Fe-Cl: range of fit 40–400 K, $\chi_0 = +1.51(4) \times 10^{-3}$ emu mol^{-1}, $\mu_{\rm eff}$/Fe atom $= 5.38\ \mu_B$, $\theta_P = -15.2(1)$ K. A similar value of 5.39 μ_B is observed for Fe-OH boracite [20]. For Fe-Br we find: range 40–400 K, $\chi_0 = +1.06(6) \times 10^{-3}$ emu mol^{-1}, $\mu_{\rm eff}$/Fe atom $= 5.51\ \mu_B$, $\theta_P = -33.9(1)$ K. For Fe-I, the analysis is limited to the range 100–170 K due to the low-lying structural PTs, which show up as weak kinks in $1/\chi(T)$. No significant term χ_0 was observed. We find: $\mu_{\rm eff}$/Fe atom $= 6.08\ \mu_B$, $\theta_P = -124(1)$ K. A Curie-Weiss fit in the range 100–400 K results in similar values.

The $\mu_{\rm eff}$ of Fe-Cl and Fe-Br are within the range for high-spin Fe^{2+} ions. For Fe-I a clearly larger value is observed, in agreement with literature ($\mu_{\rm eff}$/Fe atom $= 6.16\ \mu_B$) [164]. For the three Fe-X boracites [189] as well as for Fe-OH boracite [190] Mößbauer spectroscopy proofs that all Fe atoms are in the high-spin 2+ state and the presence of Fe^{3+} species can be excluded. Thus $\mu_{\rm eff}$ is significantly enhanced by orbital moments, as already discussed for the Ni-X and Co-X boracites. The Néel temperatures of the Fe-X boracites determined in the present study are compared with published data in Table IV. As observed for Co-X and Mn-X boracites, the AFM exchange as indicated by θ_P get stronger within the sequence Cl–Br–I. The ratio $|\theta_P|/T_N$ is small for Fe-Cl and Fe-Br boracites, only for Fe-I it attains the value of 3.72.

A. $Fe_3B_7O_{13}Cl$

The low-field magnetization $M(T)$ of Fe-Cl boracite (Fig. 23) shows a weak FM transition at $T_N = 12.05(10)$ K.

TABLE IV. Comparison of Fe-X boracite Néel temperatures T_N obtained from the specific heat peak (see Figs. 24, 26, 27) and the vanishing of the spontaneous magnetization ($H = 100$ Oe, see Fig. 23) and derived by other techniques.

T_N (K)			
Fe-Cl	Fe-Br	Fe-I	studied property and reference
11.90	18.25	32.3	specific heat peak $c_p(T)$ this work
12.05	18.5	32.8	magnetization $M(T)$ this work
11.5	15	30	magnetic susceptibility $\chi(T)$ [164]
10.5	18.4/18	30	Mößbauer effect [105,188]
		31	spont. birefringence Δn_s [186]
11.5	18.5	31	spont. magnetization M_s [112]
		31	dielectric permittivity ϵ_r' [187]

A spontaneous moment of 0.29 μ_B is measured at 1.8 K. The zero-field specific heat (Figs. 24 and 25) is characterized by a sharp peak at $T_N = 11.9$ K and a weak shoulder closely below. The shoulder may be due to anomalies analogous to the ones observed on the Co boracites, however, $M(T)$ increases in the usual manner with decreasing T. For the Co-X boracites these anomalies also show up in the ME effect (cf. Sec. VIII). Because of difficulties in preparing good single crystals and FE/FEla single domains (very high FE coercive fields) [142], no high-resolution ME effect measurements on Fe-Cl and Fe-Br are available.

The magnetic contribution $c_{\rm mag}$ of Fe-Cl does not follow a clear power law below T_N: while $c_{\rm mag} \propto T^{2.5}$ is found above 0.5 T_N a dependence $\propto T^4$ is seen below 0.4 T_N. This behavior is observed for all Fe-X boracites. The magnetic entropies $S_{\rm mag}(T)$ well above T_N of the Fe-X boracites (Fig. 24) are close to $R \ln 5$/Fe atom, as expected for the high-spin $S = 2$ state of the d^6 ion Fe^{2+}. At T_N, 56%–64% of the limiting entropy is reached, which is quite low for three-dimensional ordering [163,170].

The sharp peak at T_N is smeared out in a field of 40 kOe, however, for 90 kOe a sharp step-like transition at 11.9 K and a broad hump around 5.5 K are seen (cf. Fig. 25). $M(H)$ shows a change of slope at ≈60 kOe for increasing field and at

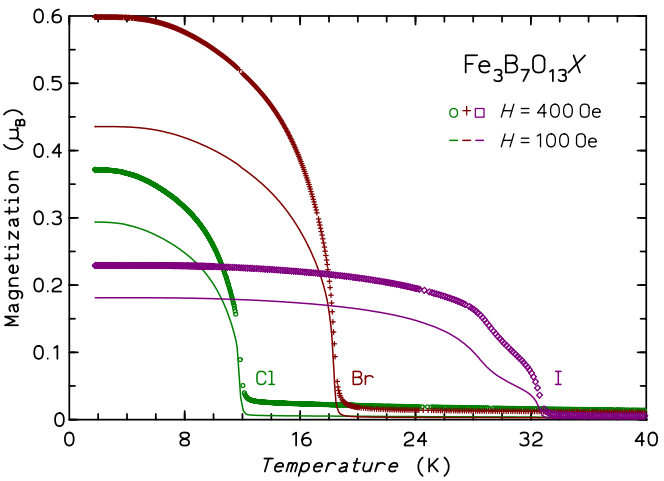

FIG. 23. (Color online) Magnetization of Fe-Cl, Fe-Br and Fe-I boracites measured during cooling in low fields.

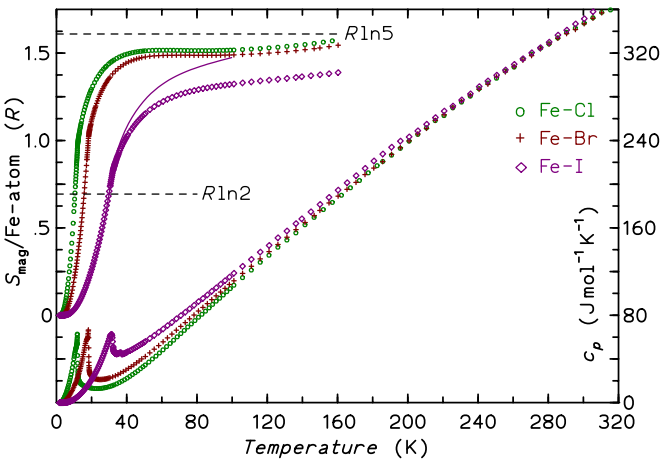

FIG. 24. (Color online) Molar heat capacity $c_p(T)$ of Fe-Cl, Fe-Br, and Fe-I boracite crystals (right axis) and magnetic entropy $S_{\rm mag}(T)$ per Fe atom (left axis).

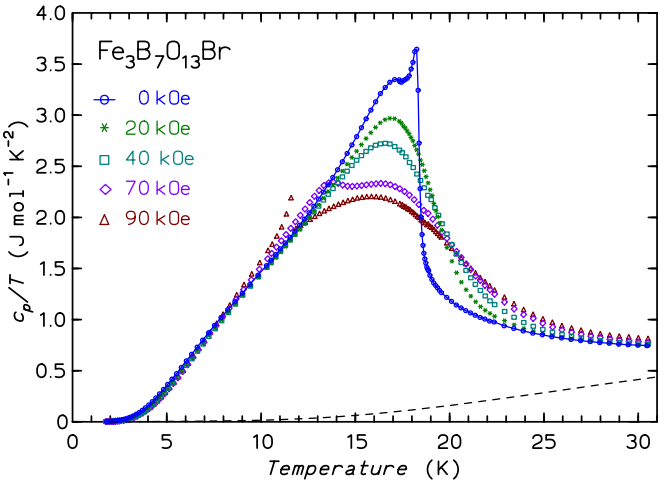

FIG. 26. (Color online) Molar heat capacity c_p/T of Fe-Br boracite in selected magnetic fields. The dashed line is the lattice contribution estimated from the Zn-Br data ($f = 0.98$).

≈50 kOe for decreasing field. These data suggest the existence of two field-induced phases.

B. $Fe_3B_7O_{13}Br$

The spontaneous magnetization of Fe-Br boracite increases below the weak FM transition at $T_N = 18.5(1)$ K in the usual manner and saturates at a value of $0.43\mu_B$ (Fig. 23). The specific heat for selected magnetic fields is shown in Fig. 26. In zero field a sharp peak marks the Néel point at 18.25(10) K. Also for Fe-Br a shoulder is observed slightly below T_N, similar to Fe-Cl. With increasing magnetic field both features are rapidly smeared out and give place to a rounded maximum which decreases in T with increasing H. In the curve for 50 kOe (not shown) a very small rounded peak appears, which gets more pronounced and decreases in T with increasing H. For $H = 70$ kOe (Fig. 26), it is located at ≈13.6 K. With further increasing field this anomaly gets sharper and finally develops to a lambda peak at 11.6 K for fields of 80–90 kOe. This anomaly indicates the crossing of a phase boundary to a field-induced phase. Interestingly, the $M(H)$ curve at 1.8 K is almost linear up to the maximum field (70 kOe). High-field studies (in and above this field range) on oriented crystals are required for the construction of a $T-H$ phase diagram. The magnetic entropy was already discussed in the previous section.

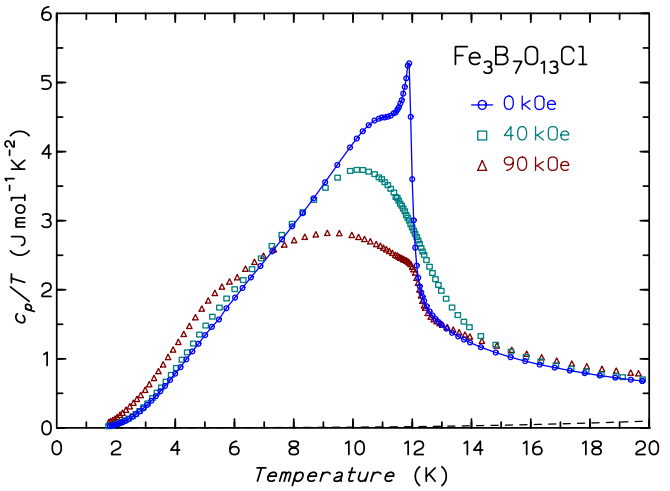

FIG. 25. (Color online) Molar heat capacity c_p/T of Fe-Cl boracite in different magnetic fields. The dashed line is the lattice contribution (Zn-Cl data scaled by $f = 0.98$).

C. $Fe_3B_7O_{13}I$

The specific heat anomaly at the Néel point of Fe-I boracite ($T_N \approx 32.3$ K, Figs. 25 and 27) is less sharp than that of Fe-Cl and Fe-Br and there is no further anomaly perceptible below T_N. This suggests that the magnetic moments on all sites order simultaneously, as found, e.g., for Mn-I [110]. However,

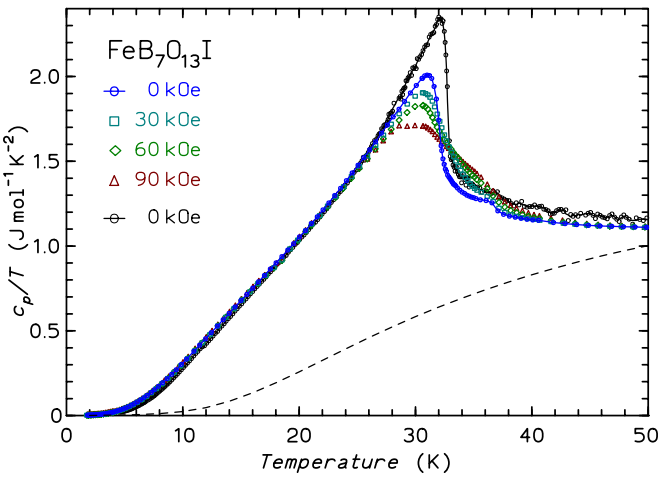

FIG. 27. (Color online) Molar heat capacity c_p/T of Fe-I boracite in different magnetic fields. The dashed line is the lattice contribution (Zn-I data). The light circles (black) connected by a line show zero-field data measured on a batch of four large crystals on the Ge2 sample holder.

the spontaneous magnetization ($T_N \approx 32.8$ K) shows a clear two-step behavior with the second step around 29 K (Fig. 23), similar to Co-I (cf. Fig. 17). Also, both the spontaneous birefringence $\Delta n_s(T)$ [186] and the spontaneous polarization $P_s(T)$ [187] do show a change in slope at 18.5 K. By forming the derivative $d\Delta n_s/dT$ in the sense of Jahn and Dachs [184], this would result in a peak of $d\Delta n_s/dT$ which might also show up in $c_p(T)$. However, since the magnetic phase of Fe-I is monoclinic, i.e., optically biaxial, the relation between $c_p(T)$ and the optical indicatrix may be more complex than in the case of optically uniaxial compounds.

The curvature of H/M between T_N and ≈100 K suggests the presence of significant short-range order well above T_N in Fe-I. This is mirrored in the magnetic specific heat $c_{\rm mag}(T)$ which is sizable even for $T \gg T_N$ (cf. background specific heat data in Fig. 27). While there is no anomaly below T_N in the $c_p(T)$ data (performed on one single crystal having mostly octahedra facets), a small steplike anomaly is observed above T_N. It coincides in temperature with a tiny step in the low-field magnetization (not shown). This small anomaly is not observed in a measurement on a larger mass of Fe-I crystals (four large specimens) on an adiabatic calorimeter. In these data (Fig. 27), the whole peak around T_N is higher but there is no trace of the feature above T_N. Measurements on better characterized and oriented crystals are required to clarify this issue.

With increasing magnetic field the specific heat peak broadens and for $H = 90$ kOe develops into two separate transitions, indicating the existence of a field-induced phase. The $M(H)$ curve at $T = 1.8$ K does not show any magnetization steps up to 70 kOe. The magnetic entropy for Fe-I was already discussed in Sec. IX A.

X. MANGANESE BORACITES

The cubic phase of the Mn-Cl, Mn-Br, and Mn-I boracites transforms into a paramagnetic FE/FEla orthorhombic phase. Measurements of the spontaneous magnetization $M_s(T)$ on the powder samples used for the calorimetric experiments gave the Néel temperatures 11.0(5) K, 14.0(5) K and 26.0(5) K for Mn-Cl, Mn-Br, and Mn-I, respectively [110]. These values compare well with 9.8, 14.1, and 26.1 K derived from $c_p(T)$ in the present work (Fig. 28). The effective magnetic moments per Mn atom ($\mu_{\rm eff} = 6.03\ \mu_B$, $5.76\ \mu_B$, $5.92\ \mu_B$) [110] are close to the spin-only value $5.92\ \mu_B$, showing the absence of orbital contributions. The (absolute) Weiss temperatures (−16.2, −26.7, −78.7 K) [110] are much higher than the respective T_N, in the case of Mn-I by a factor of 3.02.

The magnetic entropies $S_{\rm mag}(T)$ well above T_N of the Mn-X boracites reach consistently values of $R \ln 6$/Mn atom, corresponding to the $S = 5/2$ high-spin state of the three Mn^{2+} ions. The fraction of entropy reached at T_N is high and ranges between 67% (Mn-I) to 77% (Mn-Cl) of the limiting value. Also in the Mn-X boracites some short-range ordering contributions to $c_{\rm mag}(T)$ above T_N are present, but they are less pronounced than in other M-X boracites. This may be due to the essentially three-dimensional character of the exchange interactions and the high (classical) spin of the Mn^{2+} ions.

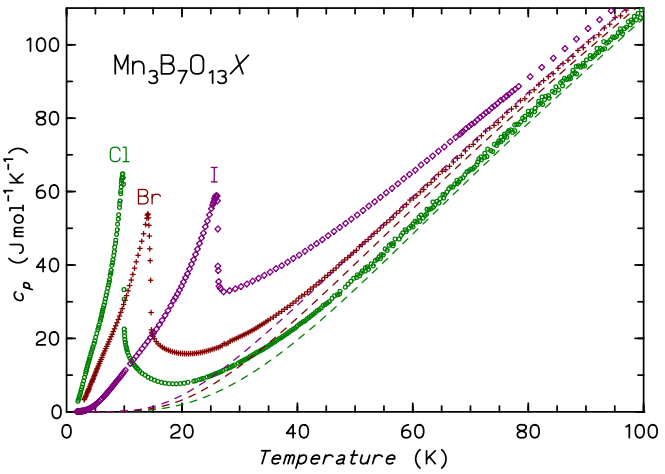

FIG. 28. (Color online) Molar heat capacity of Mn-Cl, Mn-Br, and Mn-I boracites. The dashed lines are the respective lattice contributions (data of the corresponding Zn-X boracites).

A. $Mn_3B_7O_{13}Cl$ and $Mn_3B_7O_{13}Br$

For Mn-Cl and Mn-Br the symmetry and structure of the weakly FM phase has not yet been determined. However, because of the analogous cubic ↔ orthorhombic PT and the similarity of the magnetic specific heats (Fig. 28), full analogy with Mn-I can be expected:

Mn-Cl:		$F\bar{4}3c1'(\bar{4}3m1')$
	← (683 K) [90,91] 690.3(1.0) K →	$Pca2_11'(mm21')$
	← (11 K) [110] 9.8 K →	$Pc'a2_1'(m'm2')$?
Mn-Br:		$F\bar{4}3c1'(\bar{4}3m1')$
	← (548 K) [90,91] →	$Pca2_11'(mm21')$
	← (14 K) [110] 14.2 K →	$Pc'a2_1'(m'm2')$?

For these two Mn-X boracites, single transition peaks (displaying almost the typical lambda shape) are observed in the zero-field specific heat (Fig. 29), at 9.8 K for Mn-Cl and at 14.2 K for Mn-Br. Below T_N, there are no further anomalies and $c_{\rm mag}(T)$ does not follow a particular power law. In a magnetic field of 60 kOe, the peak for Mn-Cl shifts to 9.1 K and broadens significantly. A similar broadening and a shift to 12.6 K is observed for Mn-Br in a field of 120 kOe. At least up to the measured fields, there seem to be no field-induced phases in the $T-H$ phase diagram of these boracites. This suggests, that the orbital moment of the Co^{2+} and Fe^{2+} ions is involved in the field-induced transitions of these boracites.

B. $Mn_3B_7O_{13}I$

The phase sequence in Mn-I is

	$F\bar{4}3c1'(\bar{4}3m1')$
← (404 K) [90,91] 407.4(1.0) K →	$Pca2_11'(mm21')$
← (26 K) [111] 26.1(2) K →	$Pc'a2_1'(m'm2')$.

The magnetic structure of Mn-I has been determined by neutron diffraction on a powder sample at 1.5 K [110] and refined in the magnetic space group $Pc'a2_1'$. Magnetoelectric

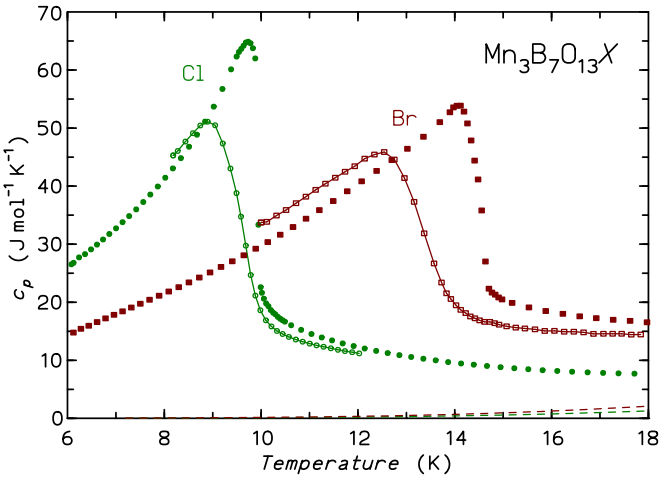

FIG. 29. (Color online) Magnetic field dependence of the molar heat capacity of Mn-Cl and Mn-Br boracites. Mn-Cl in zero (•) and 60 kOe (○ and line) magnetic field. Mn-Br in zero (■) and 120 kOe (□ and line). The dashed lines are the respective lattice contributions.

measurements and data of the spontaneous magnetization $M_s(T)$ on an orthorhombic FE/FEla single domain confirmed the neutron results, giving magnetic space group $Pc'a2'_1$, i.e., with the spontaneous magnetization lying along the orthorhombic b axis [111]. The magnetic moments of the three nonequivalent Mn sites order in a two-dimensional canted spin arrangement and the temperature dependence of the sublattice moments suggests that the spins on all sites order at T_N.

The specific heat of Mn-I (Fig. 28) shows a sharp peak at $T_N = 26.1(2)$ K. Although there is a sizable short-range ordering contribution extending to temperatures well above T_N, the critical fluctuations directly above T_N appear to be damped. The peak has not the typical lambda-shape but appears more like a step. Another observation is that at 70 K the magnetic entropy is still below $R \ln 6$. This may indicate a weakly coupled magnetostructural character of the PT. We discuss this kind of PTs in Sec. XI B on Cr-Br and Cr-I.

A weak broad hump in $c_{\rm mag}(T)$ (not shown) at $\approx$12 K becomes visible in a plot of $c_{\rm mag}/T$. Such a hump is often visible below T_N in the magnetic specific heat of compounds of ions with highly degenerate ground states as, e.g., Gd^{3+} [191], but also Mn^{2+}. In agreement with this interpretation, there are no hints for a change in the spin orientation below T_N in magnetization data ($H = 1$ kOe) along the three orthorhombic axes, nor by the dynamic ME effect [111], nor by the temperature dependence of the intensity of magnetic Bragg reflections [110].

XI. CHROMIUM BORACITES

Previous magnetic susceptibility data on powders of Cr-Cl, Cr-Br, and Cr-I boracite did not reveal any magnetic PTs but only broad maxima at low T [164]. Our data are plotted in Figs. 30(a) and 30(b), both as M/H and H/M. All three susceptibility curves show the smooth maxima, at about 26 K (Cr-Cl; 27 K [164]), 48 K (Cr-Br; 50 K [164]), and 92 K (Cr-I; 92 K [164]). Only for high T the data can be approximated by the Curie-Weiss law. Cr-Cl: range of fit

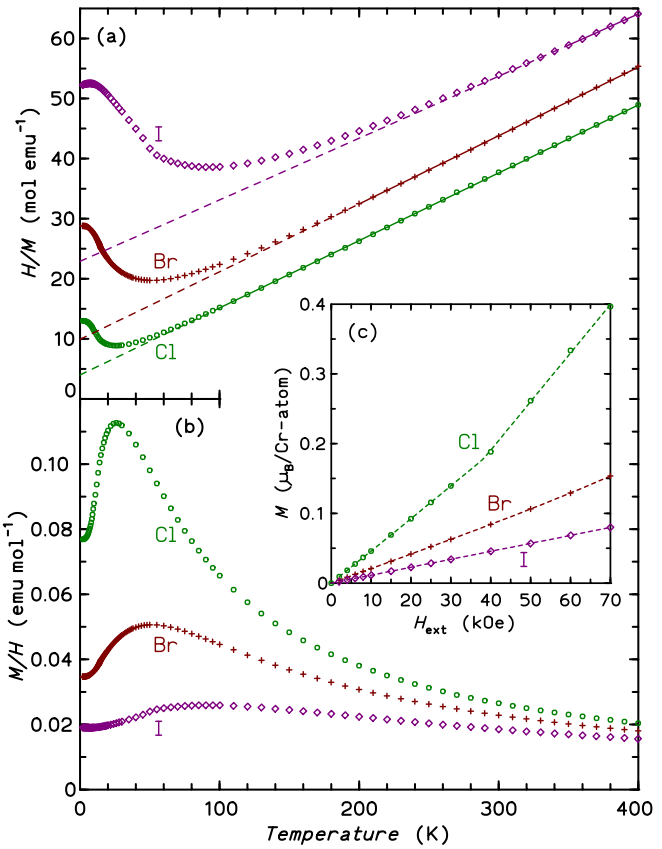

FIG. 30. (Color online) Magnetic susceptibility of polycrystalline Cr-Cl, Cr-Br, and Cr-I boracites in the representations H/M (a) and M/H (b). The Curie-Weiss fits (see text) and the extrapolations are given as full and dashed lines, respectively. (c) Isothermal magnetization curves taken in increasing field at $T = 2.0$ K.

100–400 K, $\mu_{\rm eff}$/Cr atom = 4.90 μ_B, $\theta_P = -36.0$ K. Cr-Br: range 200–400 K, $\mu_{\rm eff}$/Cr atom = 4.89 μ_B, $\theta_P = -89$ K. Cr-I: range 350–400 K, $\mu_{\rm eff}$/Cr atom = 5.14 μ_B, $\theta_P = -226$ K. The $\mu_{\rm eff}$ for Cr-Cl and Cr-Br reproduce well the spin-only value of 4.90 μ_B usually observed for octahedrally coordinated Cr^{2+} ions.

The large negative θ_P signal strong AFM interactions and the maxima in $\chi(T)$ are the hallmark of sizable frustration of these interactions. As reasoned in Sec. III, geometrical frustration is especially strong in Cr boracites: Cr-Br and Cr-I stay actually structurally cubic down to low T and the distortions in the orthorhombic (and tetragonal) phase of Cr-Cl are small [132], resulting in almost equal M-X bond distances (cf. Fig. 4). The value of $\mu_{\rm eff}$ appears to be too large for Cr-I—even with the high-temperature range of the fit and application of diamagnetic corrections. This is probably due to the extraordinary strong AFM exchange interactions and their sizable frustration, leading to such large deviations from the Curie-Weiss law.

A close inspection of high-precision susceptibility data in various fields (40 Oe–10 kOe) reveals magnetic ordering anomalies for all three Cr-X boracites. The cusps in $\chi(T)$ are unobtrusive, however, an excellent representation is obtained in the derivative $d(\chi T)/dT$ ("Fisher's heat capacity") [Fig. 31(a)], which is similar to the magnetic specific

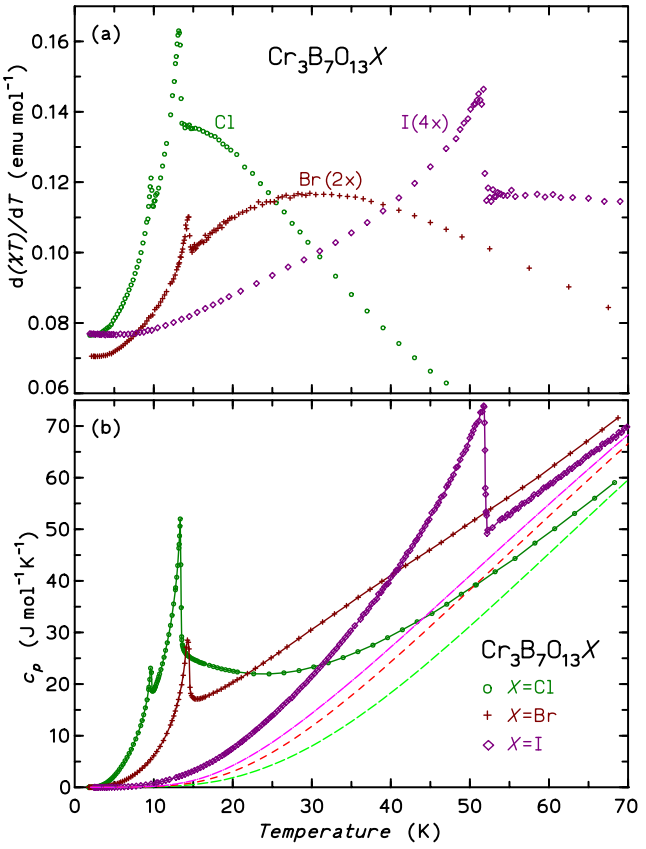

FIG. 31. (Color online) (a) Derivative $d(\chi T)/dT$ ("Fisher's heat capacity") of the magnetic susceptibility for Cr-Cl, Cr-Br and Cr-I boracite in $H = 400$ Oe. (b) Molar heat capacity (PPMS data) in the same temperature range in zero field. The lines (long-dashed, short-dashed, dash-dotted) show the estimated lattice contributions for the Cr-X boracites.

heat [183,192]. This is indeed the case, as can be seen from a comparison with the $c_p(T)$ data of the Cr-X boracites in Fig. 31(b). The anomalies in $d(\chi T)/dT$ do not vary in shape for different applied fields. No FM component could be detected in any of the magnetic phases of the Cr-X boracites, thus they are purely AFM. Figure 30(c) shows isothermal magnetization curves. Those of Cr-Br and Cr-I are linear up to the maximum field while Cr-Cl shows a kink at ≈40 kOe, eventually also indicating the beginning of a spin-flop transition.

A. $Cr_3B_7O_{13}Cl$

Cr-Cl is the only chromium boracite in which both structural and magnetic PTs occur (cf. Table I):

$$\begin{aligned} & F\bar{4}3c1'(\bar{4}3m1') \\ \leftarrow 264\ \mathrm{K} \rightarrow\ & P\bar{4}2_1c1'(2m1') \\ \leftarrow 160\ \mathrm{K} \rightarrow\ & Pca2_11'(mm21') \\ \leftarrow (13.5\ \mathrm{K})\ [42]\ 13.3\ \mathrm{K} \rightarrow\ & mm2 \\ \leftarrow (9.7\ \mathrm{K})\ [42]\ 9.6\ \mathrm{K} \rightarrow\ & m'm'2. \end{aligned}$$

The cubic phase transforms via a ferroelastic "antiferroelectric" -like tetragonal phase into a paramagnetic FE/FEla orthorhombic phase $Pca2_11'$, which undergoes a transition at $T_{N1} = 13.5$ K to an AFM FE/FEla phase with magnetic point group $mm2$ (predicted magnetic space group: $Pca2_1$) and at $T_{N2} = 9.7$ K to a FE/FEla / weakly FM group $m'm'2$ ($Pc'a'2_1$). These magnetic transitions were detected by means of a dynamic magnetoelectric $(\mathrm{ME})_H$ method, using the magnetic field induced polarization $P(H)$ along the binary axis 2 (coordinate 3) of the bilinear ME effect, $P_3 = \beta_{333}H_3^2$ [42]. The two Néel temperatures coincide with the sharp peaks in $c_p(T)$ (Figs. 31 and 32) at $T_{N2} = 9.6$ and $T_{N1} = 13.3$ K. They are also reflected, although less clearly, by anomalies of the magnetic torque [193]. In our magnetization measurements we could not detect any FM component below T_{N2}, i.e., also this phase appear to be purely AFM.

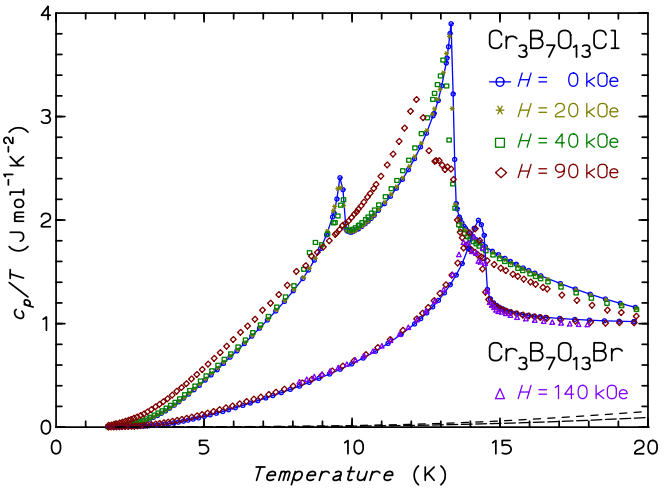

FIG. 32. (Color online) Magnetic field dependence of the molar heat capacity of Cr-Cl and Cr-Br boracites at the magnetic PTs. The long-dashed line shows the lattice heat capacity for Cr-Cl ($0.935 \times c_p$ [Zn-Cl]), the short dashed line that for Cr-Br ($0.95 \times c_p$ [Zn-Br]).

The dependence of $c_p(T)$ on magnetic fields for Cr-Cl (and Cr-Br) boracite is shown in Fig. 32. The large anomaly at T_{N1} is at $H = 90$ kOe clearly split into a step- and a peak-like anomaly at 13.3 and 12.2 K, respectively, while for $H = 40$ kOe it is still similar to the zero-field result. For $H = 40$ kOe, the small peak at T_{N2} is already split: one component remains at 9.6 K, while the other seems to be shifted to lower temperature.

The magnetic entropy at 70 K is $R \ln 5$ as expected for the $S = 2$ groundstate of the three Cr^{2+} ions [Fig. 33(b)]. Less than 40% of this value is attained at T_N since a large magnetic contribution extends far above T_{N1}. Thus, although from the ratio $|\theta_P|/T_N = 2.7$ the magnetic system appears less frustrated, the largest part of the magnetic entropy is released in short-range correlations.

B. $Cr_3B_7O_{13}Br$ and $Cr_3B_7O_{13}I$

Cr-Br and Cr-I were initially considered to remain cubic down to 4 K, because no FEla or FM domains could be detected by means of polarized light microscopy [194]. However, our magnetic susceptibility and specific heat data [Figs. 31(a), 31(b), and 32] on coarse crystalline powders clearly reveal PTs at 14.5 K and 51.8 K for Cr-Br and

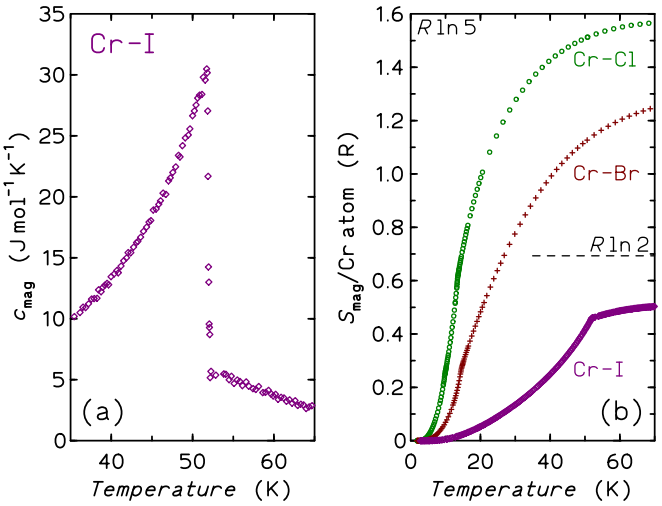

FIG. 33. (Color online) (a) Magnetic specific heat for Cr-I boracite. (b) Magnetic entropy $S_{mag}(T)$/Cr atom calculated for Cr-Cl, Cr-Br, and Cr-I boracite. The expected entropy of $R \ln 5$ lies slightly above the upper limit of the plot.

Cr-I, respectively. Polarized light microscopic observations on a $(100)_c$-cut Cr-Br plate [195] confirmed the former observations of the absence of a PT to a phase with FEla(/FE) domains, but clearly showed a pronounced growth sector structure well observable at room temperature with an optically quasitetragonal symmetry, fully analogous to that observed in Ni-I crystals [24,41].

As can be taken from the ratio $|\theta_P|/T_N$ (6.1 for Cr-Br and 4.4 for Cr-I) the AFM interactions in the cubic Cr-Br and Cr-I boracite appear to display a comparatively strong geometric frustration of magnetic exchange. These ratios are the largest among the investigated M-X boracites. For highly frustrated cubic chromium spinels [196] $ZnCr_2O_4$ and $MgCr_2O_4$, however, value $|\theta_P|/T_N$ of 25–30 are encountered. In these magnetic systems a breaking of the cubic symmetry accompanying the magnetic ordering at 12–13 K has been observed [158,197]. In $ZnCr_2O_4$ the distorted phase is tetragonal (space group $I\bar{4}m2$) with compressed c axis and displacements of the Cr ions of $\pm 9 \times 10^{-4}$ or less [198]. These magnetic transitions are weakly first order [198] and are accompanied by sizable amounts of latent heat [165,199].

From the absence of FEla domains, it can be concluded that the observed PTs in Cr-Br and Cr-I boracites are of predominantly magnetic origin, i.e., any structural distortions would have to be very small. It has to be noted that attempts at detecting by x-ray diffraction a decrease of symmetry from cubic on birefringent growth sectors of Ni-I boracite failed [200]. We can expect an analogous behavior for Cr-Br and Cr-I boracite, i.e., that the sector defect structure (Ref. [72], Sec. IIJ) does not profoundly alter the cubic structure. Taking also into account the nonobservation of FEla domains, it is plausible to attribute the specific heat peaks at 14.5 and 51.8 K to PTs from paramagnetic cubic to antiferromagnetic cubic. Then the only possible magnetic point groups are $\bar{4}3m$ and $\bar{4}'3m'$ [68]. They can in principle be distinguished by ME measurements, because $\bar{4}3m$ allows the linear ME-effect with the term of the thermodynamic potential EHH only, whereas $\bar{4}'3m'$ allows the terms EH, HEE, and EHH (see, e.g., Ref. [201]). Cubic antiferromagnetic phases are rare and of great interest, especially for their domain dynamics. Point group $\bar{4}3m$ is particularly attractive since it allows an isotropic linear ME effect (see Ref. [202], section 3.4.1.). With a view to elucidating the true magnetic symmetry, further ME experiments on Cr-Br and Cr-I boracite would be desirable.

In Cr-Br boracite the magnetic contribution to the specific heat is very small below T_N, even compared to that for Cr-Cl (see Fig. 32). The dominant magnetic contribution is a broad hump with maximum around 32 K which also shows up clearly in "Fisher's heat capacity" [cf. Figs. 31(a) and 31(b)]. Thanks to this hump the entropy $S_{mag}(T)$ reaches some 77% of the expected $R \ln 5$ at 70 K, while it attains only 16% of this value at T_N. Regarding c_{mag}/T or the magnetic entropy, the magnetic contributions are again much smaller for Cr-I than for Cr-Br [cf. Figs. 33(a) and 33(b)]. Here, only ≈30% of the expected entropy $R \ln 5$ (even much less than $R \ln 2$) is found at 70 K. Our $c_p(T)$ data for the Cr-X boracites are less accurate than those for most other compositions due to the small sample masses (cf. Ref. [72], Table I). Together with the fact that we have no suitable nonmagnetic reference data, we are unable to analyze the development of $S_{mag}(T)$ to higher temperatures, a situation observed for many systems with magnetic contributions at high temperatures. It has to be remarked that in "Fisher's heat capacity" for Cr-I, however, the maximum of the hump is passed already a few Kelvin above T_N (at ≈60 K).

Regarding the shape of the anomalies at T_N, Cr-I and, to some extent, Cr-Br boracite show a remarkably sharp decrease of $c_{mag}(T)$ on the high temperature flank, i.e., they are not lambda-type transitions as observed for purely magnetic transitions. The sharp decrease is due to the absence of the usual critical divergence of the magnetic correlation length when approaching T_N from above. It indicates that these transitions are actually of coupled magnetostructural type. No latent heat was observed at T_N for Cr-I boracite, however, the calorimetric method used is not very sensitive for latent heat.

The magnetic field dependence of $c_p(T)$ was tested at a few fields for both boracites. There is no appreciable change of T_N (max. 0.2 K downwards) in a field of 100 kOe for the Cr-I compound. For Cr-Br the results are shown in Fig. 32. In a magnetic field of 140 kOe, the peak at T_N splits, the lower flank shifts downwards by ≈0.3 K, while the upper flank does not shift. Some entropy shifts to lower T as expected for an overall AFM interaction of the Cr^{2+} ions. The influence of magnetic fields on T_N is much smaller than in other M-X boracites, corroborating the magnetostructural character of the PT. In a wide temperature interval below T_N the dependence of $c_{mag}(T)$ is $\propto T^3$ for Cr-Br (and for Cr-Cl), supporting the AFM character of the ordering.

The findings on Cr-Br and Cr-I boracites classify these magnetic systems as the strongest geometrically frustrated ones among the M-X boracites. There exist not only short-range magnetic correlations up to temperatures well above T_N, but the PTs are of magnetostructural type, where the strict geometric frustration is broken and long-range order is established at temperatures well below those expected from the exchange interactions. While $|\theta_P|/T_N$ is larger for Cr-Br than for Cr-I, the absolute energy scale is about twice in

the iodine compound. This fact may lead to the pronounced steplike shape of the c_p anomaly at T_N and possibly to a more distinct structural distortion. In contrast, since Cr-Cl orders magnetically in a structurally orthorhombic phase (with small displacements from the cubic prototype) the strict geometric frustration is already broken. Therefore the PT at T_{N1} is of lambda type, as typical for "magnetic ordering." This intriguing behavior of the Cr-X boracites deserves further investigations.

XII. MAGNETIC ORDERING AND CRYSTAL STRUCTURE OF BORACITE PHASES

Several observations and tendencies for the Néel temperature T_N, the character of the magnetic ordering, and the magnetic exchange interactions in the M-X boracites can now be correlated with features of the crystal structure, especially with the bond distances M-X, the coordination of the magnetic ion, and, especially, the degree of distortion of the environment of the magnetic species. The major observations are the following.

(1) T_N generally increases in the sequence M-Cl, M-Br, M-I. T_N increases from M-Cl to M-Br by about a factor of 1.5 for M = Mn, Fe, Co, but for the quantum-spin systems of Cu ($S = 1/2$) and Ni ($S = 1$) different ratios are observed. All chlorine boracites M-Cl have T_N around 10 K (8.6–11.85 K). These observations are easily rationalized from the increase of the lattice volume (quasicubic lattice parameter a) and of the average M-X bond distance (cf. Fig. 4) when going from M-Cl via M-Br to M-I boracites. Simple relationships between the average strength of the AFM exchange interactions (or the T_N) of M-X boracites in a sequence X = (Cl → Br → I) may be expected for M ions with classical (high) spins, however, not for Cu and Ni ions.

(2) The three investigated Co-X boracites and—to a lesser extent—the Fe-Cl, Fe-Br, and Ni-I boracites show humplike anomalies *below* T_N. We have argued that these anomalies are most probably due to continuous changes of the ordered spin arrangement (reorientation). It is also the Mn and Fe boracites where we observe several ordered phases induced by magnetic fields (in the range up to 90–140 kOe covered by our study). Obviously, orbital moment contributions are responsible for these phenomena, since they are absent in the Mn-X boracites: Mn^{2+} (d^5 high-spin) has the orbital state $L = 0$, in contrast to d^6 and d^7 ions which have high L.

(3) The magnetic specific heats of Cu-Cl, Cu-Br, and Ni-Cl boracite show small ordering peaks at T_N and broad humplike anomalies *above* T_N. The quantum-spin systems show quite large ratios $|\theta_P|/T_N$ (3.63, 3.37, and 2.49, respectively) indicating some frustration or low-dimensional character of the AFM exchange interactions. The $Pca2_11'$ structure of Ni-Cl—the exact structural parameters for Cu-Cl and Cu-Br in this structure are not yet known—at room temperature is depicted in Fig. 2. As discussed in Sec. III the Ni^{2+} (Cu^{2+}) ions are coordinated in a distorted pyramid of 4 M-O bonds and one short M-X bond. Three such compact units share a common halogen ion (cf. Fig. 2). This way, three magnetic M species form triangles with nearly equal M-M distances (in Ni-Cl 3.8541, 3.7368, and 3.8658 Å) magnetically interacting via a common halogen ion. These quite isolated triangular structures may be the origin of the magnetic frustrations in strongly distorted orthorhombic boracites (for the size of the distortions see the analysis in Fig. 4).

(4) The specific heat anomalies at T_N of Ni-I, Mn-I, Cr-Br, and especially of Cr-I boracite are not of the typical lambda-type but show a sharp decrease at high-temperature flank and a partial absence of critical magnetic fluctuations above T_N. Moreover, the T_N of Ni-I and Cr-I are remarkably higher than the T_N of corresponding bromine boracites or of other M-I boracites. The magnetic ordering in these boracite compounds takes place either in a cubic (Ni-I, Cr-Br, Cr-I; cf. the cubic structure of Cu-Br boracite, Fig. 1) or in very weakly distorted phases (examples: Mn-I, Cr-Cl). The arrangement of the magnetic M^{2+} ions in the cubic phase leads to sizable frustration for AFM superexchange interactions via the halogen atoms. Breaking of this frustration leads to magnetic ordering and (presumably very weak) structural distortions via coupled *magnetostructural* PTs (Sec. XI B). Since no latent heat could be observed at the PTs, the structural distortions should be very small. The most sizable distortions may be expected for Ni-I and Cr-I which display the strongest AFM exchange interactions among the investigated boracites (highest absolute Weiss temperatures $|\theta_P|$). However, the magnetostructural character of the transitions leads to the above-mentioned characteristic shape of the c_p anomalies of these boracites.

XIII. SUMMARY AND OUTLOOK

The boracites of the 3d transition metals display a wealth of structural ferroelectric/ferroelastic phases at elevated temperature and magnetic ordering phenomena at low temperature (see Table I and Ref. [76], Table III). The latter are determined by the magnetic species and the details of the structure. Frustration of magnetic superexchange interactions is weak in boracites and originates from different structural features. The investigated series of boracite compounds spans from the quantum spin ions Cu^{2+} and Ni^{2+} to classical spin systems (Mn^{2+} ion). They are type-I [65] multiferroic substances par excellence, some of them permitting all four primary ferroic properties.

Experimental access to the exact physical properties of the multiferroic phases of the M-X boracites, however, still faces extraordinary difficulties due to the formation of ferroelectric/ferroelastic domains in the crystals. The here presented results of heat capacity measurements give a more integral view on the properties of the magnetically ordered phases. Our specific heat data in magnetic fields indicate the existence of several field-induced phases, especially in the Co and Fe boracites, however, further investigation requires work on single-domain crystals.

While the structural sequences for the M-X boracites with M = Cr–Zn and X = (Cl, Br, I) appear to be settled by now on the level of point groups, exact nuclear or magnetic spin structures are known for only a few low-temperature phases. We think that with the present study a comprehensive overview on the magnetic and thermal properties of the investigated M-X (X = Cl, Br, I) boracites is reached, however, due to the large number of compounds, several details could not be addressed and numerous questions open up. For further

experimental investigations, especially of the anisotropic magnetic properties of noncubic boracites, single FE/FEla domains of sufficient size are desirable. The preparation and measurement of such specimens is essential for a meaningful discussion of the magnetic phase diagrams in high magnetic fields (most previous magnetooptical studies of magnetoelectic effects on microscopic domains were limited to magnetic fields of typically 10 kOe [43]).

Moreover, boracites compounds with F, OH, or NO_3 anions [10,11,22,203–205], have been prepared, but not much is known about the low-temperature structural transitions (and nothing at all on the corresponding magnetic transitions and phases). An exception is a recent magnetic properties study of a new Fe-OH boracite [20,21]. Therefore, even several decades after the first syntheses of transition-metal halogen (*M*-*X*) boracite species and the first observation of the phenomenon of multiferroic ordering in Ni-I boracite (in the year 1966), the transition-metal boracites are a particulary wide and attractive subject for the exploration of multiferroic properties as well as for studies in magnetic spin systems.

ACKNOWLEDGMENTS

We are grateful to E. Gmelin for support and discussions in the early stage of this work at MPI-FKF. Also we thank R. Kniep for support at MPI-CPfS. The assistance of E. Schmitt, K. Ripka, and R. Koban is acknowledged. The authors thank S. Leipe, U. Schwarz, and M. Schmidt for their high-pressure experiments in order to obtain Cu-I boracite material, the only *M*-*X* boracite missing in the present study. W.S. thanks H. Rosner for discussions and a preliminary DFT calculation. We are grateful to J.-P. Rivera and A. Leithe-Jasper for critical reading of the manuscript. H.S. thanks the MPI-CPfS for invited stays. Partial support by the Swiss National Science Foundation is gratefully acknowledged.

[1] G. S. O. Lasius, Chemische Annalen (of L. F. F. Crell) **1787** II, 333 (1787).
[2] A. G. Werner and C. A. G. Hoffmann, in *Bergmännisches Journal*, edited by A. W. Köhler (Craz, Freiberg, 1789), Vol. 2 (Band 1), pp. 378, 393–4.
[3] The interesting early history of boracite is detailed in G. H. O. Volger, *Versuch einer Monographie des Borazites* (Carl Rümpler, Hannover, 1855). Some remarks on later developments can be found in Ref. [84].
[4] R. J. Haüy, J. Phys. (Paris) **38**, 323 (1791).
[5] J. Curie and P. Curie, Bull. Soc. Min. France **3**, 90 (1880).
[6] As common in the literature, we abbreviate the boracites by their constituents *M*-*X* in this work.
[7] T. Mitsui, S. Nomura, and M. Adachi, in *Landolt-Börnstein, New Series, Group III: vol. 16a*, edited by K.-H. Hellwege and A. M. Hellwege (Springer-Verlag, Berlin, 1981), pp. 261–623.
[8] E. Nakamura *et al.*, in *Landolt-Börnstein, New Series, Group III: Vol. 28b*, edited by O. Madelung (Springer-Verlag, Berlin, 1990).
[9] E. Burzo, in *Landolt-Börnstein, New Series, Group III: Vol. 27h*, edited by H. P. J. Wijn (Springer-Verlag, Berlin, 1993), pp. 128–204.
[10] T. A. Bither and H. S. Young, J. Solid State Chem. **10**, 302 (1974).
[11] U. Werthmann, H. Gies, J. Glinnemann, and Th. Hahn, Z. Kristallogr. **215**, 393 (2000).
[12] J. W. Anthony, R. A. Bideaux, K. W. Bladh, and M. C. Nichols, *Handbook of Mineralogy*, (Mineral Data Publishing, Tucson AZ, 2003), Vol. 5, www.handbookofmineralogy.org.
[13] T. Ito, N. Morimoto, and R. Sadanaga, Acta Crystallogr. **4**, 310 (1951).
[14] S. Sueno, J. R. Clark, J. J. Papike, and J. A. Konnert, Am. Mineral. **58**, 691 (1973).
[15] E. Dowty and J. R. Clark, Z. Kristallogr. **138**, 64 (1973).
[16] P. C. Burns and M. A. Carpenter, Can. Mineral. **34**, 881 (1996).
[17] R. M. Honea and F. R. Beck, Am. Mineral. **47**, 665 (1962).
[18] A. Levasseur, B. Rouby, and C. Fouassier, C. R. Acad. Sci. (Paris) **277**, 421 (1973).
[19] W. Jeitschko, T. A. Bither, and P. E. Bierstedt, Acta Crystallogr. Sec. B **33**, 2767 (1977).
[20] I. Nomoto, H. Sato, T. Fukui, Y. Narumi, K. Kindo, S. Nakamura, and Y. Tsunoda, J. Phys. Soc. Jpn. **80**, 014801 (2011).
[21] G. Nénert, I. Nomoto, and H. Sato, arXiV:1410.6602v1.
[22] S. C. Neumair, J. S. Knyrim, O. Oeckler, R. Kaindl, and H. Huppertz, Z. Naturforsch. B **66**, 107 (2011).
[23] E. Ascher, H. Rieder, H. Schmid, and H. Stössel, J. Appl. Phys. **37**, 1404 (1966).
[24] H. Schmid, Rost Kristallov **7**, 32 (1967) [Crystal Growth **7**, 25 (1969)].
[25] H. Schmid, Ferroelectrics **427**, 1 (2012).
[26] P. Curie, J. Phys. Théor. Appl. **3**, 393 (1894), Reprinted in "*Oevres de Pierre Curie*" (Gauthier-Villars, Paris, 1908).
[27] T. H. O'Dell, *The Electrodynamics of Magneto-Electric Media* (North-Holland, Amsterdam, London, 1970).
[28] A. J. Freeman and H. Schmid (eds.), *Magnetoelectric Interaction Phenomena in Crystals* (Gordon and Breach Science Publishers, London, New York, Paris, 1975).
[29] *Proceedings of 2nd International Conference on Magnetoelectric Interaction Phenomena in Crystals (MEIPIC-2) (Ascona, 1993)*, edited by H. Schmid, A. Janner, H. Grimmer, J.-P. Rivera, and Z.-G. Ye, in *Ferroelectrics*, Vol. 161 [Part I] and Vol. 162 [Part II] (Taylor and Francis, London, 1994).
[30] *Proceedings of 3rd International Conference on Magnetoelectric Interaction Phenomena in Crystals (MEIPIC-3)*, edited by M. Bichurin, in *Ferroelectrics*, Vol. 204, Numbers 1-4 (Taylor and Francis, London, 1997).
[31] *Proceedings of 4th International Conference on Magnetoelectric Interaction Phenomena in Crystals (MEIPIC-4)*, edied by M. Bichurin, in *Ferroelectrics*, Vol. 279 and Vol. 280 (Taylor and Francis, London, 2002).
[32] *Magnetoelectric Interaction Phenomena in Crystals (MEIPIC-5)*, edited by M. Fiebig, V. Eremenko, and I. Chupis (Kluver, Dordrecht, 2004).
[33] M. Fiebig and N. A. Spaldin, Eur. Phys. J. B **71**(3), 293 (2009).

[34] H. Schmid, in *Magnetoelectric Interaction Phenomena in Crystals (MEIPIC-5)*, edited by M. Fiebig, V. Eremenko, and I. Chupis (Kluver, Dordrecht, 2004), pp. 1–34.
[35] G. A. Smolensky and I. E. Chupnis, Sov. Phys. Usp. **25**, 475 (1982).
[36] H. Schmid, in *Introduction to Complex Mediums for Optics and Electromagnetics*, edited by W. S. Weiglhofer and A. Lakhtakia (SPIE Press, Bellingham, WA, 2003), pp. 167–95.
[37] N. A. Hill, J. Phys. Chem. B **104**, 6694 (2000).
[38] M. Fiebig, J. Phys. D: Appl. Phys. **38**, R123 (2005).
[39] N. A. Spaldin and M. Fiebig, Science **309**, 391 (2005).
[40] H. Schmid, J. Phys. Condens. Matter **20**, 434201 (2008).
[41] H. Schmid, Ferroelectrics **162**, 317 (1994).
[42] J.-P. Rivera, Ferroelectrics **161**, 165 (1994).
[43] J.-P. Rivera, Eur. Phys. J. B **71**, 299 (2009).
[44] A. S. Borovik-Romanov, H. Grimmer, and M. Kenzelmann, in *International Tables for Crystallography*, 2nd ed., edited by A. Authier (International Union of Crystallography, Geneva, Switzerland, 2013), Vol. D, Chap. 1.5.8, pp. 139–145, http://it.iucr.org.
[45] J.-P. Rivera and H. Schmid, Ferroelectrics **36**, 447 (1981).
[46] H. Schmid, Ferroelectrics **221**, 9 (1999).
[47] B. B. Van Aken, J.-P. Rivera, H. Schmid, and M. Fiebig, Nature (London) **449**, 702 (2007).
[48] A. A. Gorbatsevich and Y. V. Kopaev, Ferroelectrics **161**, 321 (1994).
[49] V. M. Dubovik and V. V. Tugushev, Phys. Rep. **187**, 145 (1990).
[50] H. Schmid, Ferroelectrics **252**, 1 (2001).
[51] N. A. Spaldin, M. Fiebig, and M. Mostovoy, J. Phys. Condens. Matter **20**, 434203 (2008).
[52] C. Ederer and N. A. Spaldin, Phys. Rev. B **76**, 214404 (2007).
[53] E. Ascher, Int. J. Magn. **5**, 287 (1974).
[54] D. G. Sannikov and I. S. Zhedulev, Fiz. Tverd. Tela (Leningrad) **27**, 1369 (1985) [Sov. Phys. Solid State **27**, 826 (1985)].
[55] D. G. Sannikov, Zh. Eksp. Teor. Fiz. **111**, 536 (1997) [JETP **84**, 293 (1997)].
[56] D. G. Sannikov, Ferroelectrics **219**, 177 (1998).
[57] D. G. Sannikov, Pis'ma Zh. Eksp. Teor. Fiz. **73**, 447 (2001) [JETP Lett. **73**, 401 (2001)].
[58] D. G. Sannikov, Ferroelectrics **291**, 157 (2003).
[59] D. G. Sannikov, Ferroelectrics **291**, 163 (2003).
[60] D. I. Khomskii, J. Magn. Magn. Mater. **306**, 1 (2006).
[61] W. Eerenstein, N. D. Mathur, and J. F. Scott, Nature (London) **442**, 759 (2006).
[62] Y. Tokura, J. Magn. Magn. Mater. **310**, 1145 (2007).
[63] S.-W. Cheong and M. Mostovoy, Nat. Mater. **6**, 13 (2007).
[64] A. P. Pyatakov and A. K. Zvezdin, Phys. Usp. **55**, 557 (2012).
[65] D. Khomskii, Physics **2**, 20 (2009).
[66] E. Ascher, Helv. Phys. Acta **39**, 40 (1966).
[67] V. Dubovik, S. S. Krotov, and V. V. Tusgushev, Kristallografiya **32**, 540 (1987) [Sov. Phys. Crystallogr. **32**, 314 (1987)].
[68] K. Aizu, Phys. Rev. B **2**, 754 (1970).
[69] D. B. Litvin, Acta Crystallogr. Sect. A **64**, 316 (2008).
[70] Y. F. Popov, A. M. Kadomtseva, G. P. Vorob'ev, V. A. Timofeeva, D. M. Ustinin, A. K. Zvezdin, and M. M. Tegeranchi, Zh. Eksp. Teor. Fiz. **114**, 263 (1998) , JETP **87**, 146 (1998)].
[71] R. Villar, E. Gmelin, and S. Vieira, Solid State Commun. **38**, 807 (1981).
[72] See Supplemental Material at http://link.aps.org/supplemental/10.1103/PhysRevB.91.184411 for details of the calorimetric methods (section I) and the results on the structural phase transitions of the investigated M-X boracites (Sec. II). Section III contains four tables. In Table I, information on the samples is collected, Table II gives the thermodynamic standard values, Table III summarizes the sequences and temperatures of the phase transitions, and Table IV presents a collection of thermodynamic data determined at the structural phase transitions from the literature.
[73] W. Schnelle and E. Gmelin, Thermochim. Acta **391**, 41 (2002).
[74] W. Schnelle and E. Gmelin, Thermochim. Acta **269-270**, 27 (1995).
[75] W. Schnelle, J. Engelhardt, and E. Gmelin, Cryogenics **39**, 271 (1999).
[76] V. M. Gurevich, V. E. Gorbunov, K. S. Gavrichev, T. D. Aksenova, and I. L. Khodakovskii, Geokhimiya **38**, 676 (2000) [Geochemistry International **38**, 615 (2000)].
[77] B. G. Bochkov, N. D. Gavrilova, V. K. Novik, and V. K. Koptsik, Kristallografiya **20**, 659 (1975) [Sov. Phys. Crystallogr. **20**, 404 (1975)].
[78] H. Schmid, Battelle-Geneva report, 1975 (unpublished).
[79] K. K. Kelley, Contribution to the Data on Theoretical Metallurgy. II. High-Temperature Specific-Heat Equations for Inorganic Substances, Bur. Mines Bull. **371**, 33 (1934).
[80] E. Mallard, Bull. Soc. Min. France **6**, 122 (1883).
[81] K. Kroeker, Nachr. K. Ges. Wiss. Göttingen **1892**, 122 (1892).
[82] J.-P. Rivera, Ferroelectrics **21**, 455 (1978).
[83] M. Delfino, G. M. Loiacono, W. A. Smith, and P. S. Gentile, J. Solid State Chem. **33**, 107 (1980).
[84] H. Schmid and H. Tippmann, Ferroelectrics **20**, 21 (1978).
[85] J.-F. Rossignol, J.-P. Rivera, and H. Schmid, Jpn. J. Appl. Phys. **24**, Suppl. 24-2, 574 (1985).
[86] M. Senthil Kumar, J.-P. Rivera, Z.-G. Ye, S. D. Gentil, and H. Schmid, Ferroelectrics **204**, 57 (1997).
[87] F. Smutný, Phys. Status Solidi A **9**, K109 (1972).
[88] B. G. Bochkov, V. I. Bugakov, N. D. Gavrilova, V. K. Koptsik, and V. K. Novik, Kristallografiya **17**, 1250 (1972) [Sov. Phys. Crystallogr. **17**, 1093 (1972)].
[89] H. Schmid, P. Chan, L. A. Pétermann, F. Teufel, and M. Mändly, Ferroelectrics **13**, 351 (1976).
[90] A. G. Castellanos-Guzmán, J. Solid State Chem. **54**, 78 (1984).
[91] A. G. Castellanos-Guzmán, J. C. Burfoot, H. Schmid, and P. Tissot, Ferroelectrics **36**, 411 (1981).
[92] M.-E. Mendoza-Alvarez, J.-P. Rivera, H. Schmid, and G. Wildermuth, Ferroelectrics **55**, 213 (1984).
[93] P. Tissot, J. Painot, J.-P. Rivera, and H. Schmid, Thermochim. Acta **56**, 359 (1982).
[94] S.-Y. Mao, M.-E. Mendoza-Alvarez, W. Depmeier, F. Kubel, H. Schmid, and K. Yvon, Ferroelectrics **115**, 91 (1991).
[95] P. Félix, M. Lambert, R. Comès, and H. Schmid, Ferroelectrics **7**, 131 (1974).
[96] T. I. Nedoseykina, V. A. Shuvaeva, I. V. Pirog, A. T. Shuvaev, K. Yagi, Y. Azuma, and H. Terauchi, Ferroelectrics **284**, 175 (2003).
[97] J. Pascual, J. Íñiguez, M. N. Iliev, V. G. Hadjiev, and J. Meen, Phys. Rev. B **79**, 104115 (2009).
[98] Z.-G. Ye, J.-P. Rivera, and H. Schmid, Ferroelectrics **116**, 251 (1991).
[99] H. Schmid, J. Phys. Chem. Solids **26**, 973 (1965).
[100] H. Schmid and H. Tippmann, J. Cryst. Growth **46**, 723 (1979).

[101] J. G. Hannes, L. Perillo, M. E. Rosar, and A. Shaulov (1981), Electrical and thermal properties of nickel bromine and mixed nickel bromine chlorine boracites, Philips Laboratories, Briarcliff Manor, New York, Report No. 385.
[102] M. N. Iliev and H. Schmid, J. Raman Spectrosc. **45**, 267 (2014).
[103] B. Kahr and J. M. McBride, Angew. Chem., Int. Ed. Engl. **31**, 1 (1992).
[104] F. Rinne, N. Jb. Mineral. Geol. Paläont. **2**, 108 (1900).
[105] P. Tolédano, H. Schmid, M. Clin, and J.-P. Rivera, Phys. Rev. B **32**, 6006 (1985).
[106] M. Clin, J.-P. Rivera, and H. Schmid, Ferroelectrics **108**, 207 (1990).
[107] T. Lottermoser, D. Meier, R. V. Pisarev, and M. Fiebig, Phys. Rev. B **80**, 100101(R) (2009).
[108] Y. J. Choi, J. Okamoto, D. J. Huang, K. S. Chao, H. J. Lin, C. T. Chen, M. van Veenendaal, T. A. Kaplan, and S.-W. Cheong, Phys. Rev. Lett. **102**, 067601 (2009).
[109] Z.-G. Ye, J.-P. Rivera, and H. Schmid, Ferroelectrics **106**, 87 (1990).
[110] O. Crottaz, P. Schobinger-Papamantellos, E. Suard, C. Ritter, S. Gentil, J.-P. Rivera, and H. Schmid, Ferroelectrics **204**, 45 (1997).
[111] O. Crottaz, J.-P. Rivera, B. Revaz, and H. Schmid, Ferroelectrics **204**, 125 (1997).
[112] D. Andreica, J.-P. Rivera, S. Gentil, Z.-G. Ye, M. Senthil Kumar, and H. Schmid, Ferroelectrics **204**, 73 (1997).
[113] M. Clin, J.-P. Rivera, and H. Schmid, Helv. Phys. Acta **60**, 287 (1987).
[114] M. Clin, J.-P. Rivera, and H. Schmid, Ferroelectrics **108**, 213 (1990).
[115] M. Haida, K. Kohn, and H. Schmid, J. Phys. Soc. Jpn. **37**, 1463 (1974).
[116] J.-P. Rivera and H. Schmid, J. Appl. Phys. **70**, 6410 (1991).
[117] J.-P. Rivera, F. J. Schäfer, W. Kleemann, and H. Schmid, Jpn. J. Appl. Phys. **24**, Suppl. 24-2, 1060 (1985).
[118] M. Haida, K. Kohn, and J. Kobayashi, J. Phys. Soc. Jpn. **39**, 1625 (1975).
[119] J.-P. Rivera and H. Schmid, J. Phys. Colloques **49**, C8-849 (1988).
[120] G. Berset, Ph.D. thesis, University of Geneva, 1989.
[121] C. Berger, M. Richard, and L. Eyraud, Bull. Soc. Chim. France Mémoire No. 224, 1491 (1965).
[122] F. Smutný, Phys. Status Solidi A **50**, K201 (1978).
[123] H. Schmid, Battelle-Geneva report, 1977 (unpublished).
[124] W. Schnelle, E. Gmelin, O. Crottaz, and H. Schmid, J. Therm. Anal. Cal. **56**, 365 (1999).
[125] M. Clin, W. Dai, E. Gmelin, and H. Schmid, Ferroelectrics **108**, 201 (1990).
[126] As for the magnetization, the specific heat in magnetic fields depends in principle on the direction of the field in the crystal coordinate system.
[127] In the used MPMS magnetometer, the real field is usually some 5 Oe lower, resulting, e.g., in a lower susceptibility for nominal fields of 100 Oe compared to 2-kOe data. Since we cannot not measure the real field at each field change we did not correct the results for this effect.
[128] R. J. Nelmes and W. J. Hay, J. Phys. C **14**, 5247 (1981).
[129] F. Kubel, S.-Y. Mao, and H. Schmid, Acta Crystallogr. Sect. C **48**, 1167 (1992).
[130] M. Yoshida, K. Yvon, F. Kubel, and H. Schmid, Acta Crystallogr. Sect. B **48**, 30 (1992).
[131] F. Kubel and O. Crottaz, Z. Kristallogr. **211**, 926 (1996).
[132] S.-Y. Mao, F. Kubel, H. Schmid, and K. Yvon, Ferroelectrics **132**, 239 (1992).
[133] K. Knorr, L. Peters, B. Winkler, V. Milman, and A. G. Castellanos-Guzmán, J. Phys. Condens. Matter **19**, 275207 (2007).
[134] R. D. Shannon, Acta Crystallogr. Sect. A **32**, 751 (1976).
[135] L. P. Torre, S. Abrahams, and R. L. Barns, Ferroelectrics **4**, 291 (1971).
[136] H. Schmid, G. Kliegl, and J. Kobayashi, Helv. Phys. Acta **42**, 599 (1969).
[137] R. J. Nelmes, J. Phys. C **7**, 3840 (1974).
[138] A. Monnier, G. Berset, H. Schmid, and K. Yvon, Acta Crystallogr. Sect. C **43**, 1243 (1987).
[139] F. Kubel and O. Crottaz, Z. Kristallogr. **211**, 924 (1996).
[140] F. Kubel and O. Crottaz, Z. Kristallogr. **211**, 925 (1996).
[141] M.-E. Mendoza-Alvarez, K. Yvon, W. Depmeier, and H. Schmid, Acta Crystallogr. Sect. C **41**, 1551 (1985).
[142] H. Schmid, Phys. Status Solidi **37**, 209 (1970).
[143] V. A. Shuvaeva, K. A. Lysenko, and M. Y. Antipin, Kristallografiya **56**, 1073-1075 (2011) [Cryst. Reports **56**, 1004 (2011)].
[144] F. Kubel and A.-M. Janner, Acta Crystallogr. Sect. C **49**, 657 (1993).
[145] S. C. Abrahams, J. L. Bernstein, and C. Svensson, J. Chem. Phys. **75**, 1912 (1981).
[146] R. J. Nelmes and F. R. Thornley, J. Phys. C **9**, 665 (1976).
[147] G. Berset, W. Depmeier, R. Boutellier, and H. Schmid, Acta Crystallogr. Sect. C **41**, 1694 (1985).
[148] W. J. Deiss and P. Blum, C. R. Acad. Sci. (Paris) **244**, 464 (1957).
[149] M. Clin, H. Schmid, P. Schobinger, and P. Fischer, Phase Transitions **33**, 149 (1991).
[150] F. Kubel, Ferroelectrics **160**, 61 (1994).
[151] S.-Y. Mao, F. Kubel, H. Schmid, P. Schobinger, and P. Fischer, Ferroelectrics **146**, 81 (1993).
[152] F. R. Thornley, N. S. J. Kennedy, and R. J. Nelmes, J. Phys. C **9**, 681 (1976).
[153] J. Campa-Molina, S. Ulloa-Godínez, A. Barrera, L. Bucio, and J. Mata, J. Phys. Condens. Matter **18**, 4827 (2006).
[154] P. Schiffer and A. P. Ramirez, Comments Condens. Matter Phys. **18**, 21 (1996).
[155] A. P. Ramirez, in *Handbook on Magnetic Materials*, edited by K. H. J. Buschow (Elsevier, Amsterdam, 2001), Vol. 13, pp. 423–520.
[156] J. E. Greedan, J. Mater. Chem. **11**, 37 (2001).
[157] *Introduction to Frustrated Magnetism*, edited by C. Lacroix, P. Mendels, and F. Mila, Springer Series in Solid-State Sciences Vol. 164 (Springer, Berlin, 2011).
[158] S.-H. Lee, C. Broholm, T. H. Kim, W. Ratcliff, and S.-W. Cheong, Phys. Rev. Lett. **84**, 3718 (2000).
[159] E. S. R. Gopal, *Specific Heat at Low Temperatures* (Plenum Press, London, 1966).
[160] A. Tari, *The Specific Heat of Matter at Low Temperatures* (Imperial College Press, London, 2003).
[161] T. H. K. Barron and G. K. White, *Heat Capacity and Thermal Expansion at Low Temperatures* (Kluver Academic/Plenum Publishers, New York, 1999).

[162] P. W. Selwood, *Magnetochemistry*, 2nd ed. (Interscience, New York, 1956).
[163] R. L. Carlin, *Magnetochemistry* (Springer, Berlin, 1986).
[164] G. Quèzel and H. Schmid, Solid State Commun. **6**, 447 (1968).
[165] W. Schnelle *et al.* (unpublished).
[166] H. Schmid, H. Rieder, and E. Ascher, Solid State Commun. **3**, 327 (1965).
[167] S.-Y. Mao, H. Schmid, G. Triscone, and J. Muller, J. Magn. Magn. Mater. **195**, 65 (1999).
[168] J.-P. Rivera, H. Schmid, J. M. Moret, and H. Bill, Int. J. Magn. **6**, 221 (1974).
[169] Z.-G. Ye, P. Schobinger-Papamantellos, S.-Y. Mao, C. Ritter, E. Suard, M. Sato, and H. Schmid, Ferroelectrics **204**, 83 (1997).
[170] L. J. de Jongh and A. R. Miedema, Adv. Phys. **23**, 1 (1974), republished: **50**, 947 (2001).
[171] J.-P. Rivera and H. Schmid, Ferroelectrics **55**, 295 (1984).
[172] I. H. Brunskill and H. Schmid, Ferroelectrics **36**, 395 (1981).
[173] S.-Y. Mao, J.-P. Rivera, and H. Schmid, Ferroelectrics **141**, 141 (1993).
[174] W. von Wartburg, Phys. Status Solidi A **21**, 557 (1974).
[175] J.-P. Rivera and H. Schmid, Ferroelectrics **42**, 35 (1982).
[176] M. Clin, J.-P. Rivera, and H. Schmid, Jpn. J. Appl. Phys. **24**, 1054 (1985).
[177] M. Clin, J.-P. Rivera, and H. Schmid, Ferroelectrics **79**, 173 (1988).
[178] L. N. Baturov, R. V. Zorin, B. I. Al'shin, and V. I. Bugakov, Fiz. Tverd. Tela (Leningrad) **23**, 908 (1981) [Sov. Phys. Solid State **23**, 525 (1981)].
[179] M.-E. Mendoza-Alvarez, J.-P. Rivera, and H. Schmid, Jpn. J. Appl. Phys. **24**, 1057 (1985).
[180] P. Schobinger-Papamantellos, Z.-G. Ye, H. Schmid, C. Ritter, and E. Suard (unpublished).
[181] P. Schobinger-Papamantellos, P. Fischer, F. Kubel, and H. Schmid, Ferroelectrics **162**, 93 (1994).
[182] O. Kahn, *Molecular Magnetism* (Wiley VCH, Weinheim, 1993).
[183] J. Skalyo, Jr., A. F. Cohen, S. A. Friedberg, and R. B. Griffith, Phys. Rev. **164**, 705 (1967).
[184] I. R. Jahn and H. Dachs, Solid State Commun. **9**, 1617 (1971).
[185] J. Ferré and G. A. Gehring, Rep. Prog. Phys. **47**, 513 (1984).
[186] Z.-G. Ye, A. M. Janner, J.-P. Rivera, and H. Schmid, Ferroelectrics **141**, 135 (1993).
[187] Z.-G. Ye, A.-M. Janner, and H. Schmid, J. Phys. Condens. Matter **9**, 2607 (1997).
[188] R. Jagannathan, J. M. Trooster, and M. P. A. Viegers, Int. J. Magn. **4**, 363 (1973).
[189] H. Schmid and J. M. Trooster, Solid State Commun. **5**, 31 (1967).
[190] S. Nakamura, Y. Tsunoda, I. Nomoto, and H. Sato, Hyperfine Interact. **197**, 101 (2010).
[191] U. Köbler, D. Hupfeld, W. Schnelle, K. Mattenberger, and T. Brückel, J. Magn. Magn. Mater. **205**, 90 (1999).
[192] M. E. Fisher, Philos. Mag. **7**, 1731 (1962).
[193] Z.-G. Ye, J.-P. Rivera, H. Schmid, M. Haida, and K. Kohn, Ferroelectrics **161**, 99 (1994).
[194] H. Schmid (unpublished).
[195] J.-P. Rivera and H. Schmid, Observation of growth sectors in Cr-Br boracite down to 4 K (unpublished).
[196] H. Takagi and S. Niitaka, in *Introduction to Frustrated Magnetism*, edited by C. Lacroix, P. Mendels, and F. Mila, Springer Series in Solid-State Sciences Vol. 164 (Springer, Berlin, 2011), pp. 155–175.
[197] H. Ehrenberg, M. Knapp, C. Baehtz, and S. Klemme, Powder Diffr. **17**, 230 (2002).
[198] S. Ji, S.-H. Lee, C. Broholm, T. Y. Koo, W. Ratcliff, S.-W. Cheong, and P. Zschack, Phys. Rev. Lett. **103**, 037201 (2009).
[199] S. Klemme, H. S. O'Neill, W. Schnelle, and E. Gmelin, Am. Mineral. **85**, 1686 (2000).
[200] R. J. Nelmes and F. R. Thornley, Ferroelectrics **13**, 355 (1976).
[201] H. Schmid, Int. J. Magn. **4**, 337 (1973).
[202] F. W. Hehl, Y. N. Obukhov, J.-P. Rivera, and H. Schmid, Eur. Phys. J. B **71**, 321 (2009).
[203] J. C. Joubert, J. Muller, C. Fouassier, and A. Levasseur, Kristall Techn. (Crystal Res. Technol.) **6**, 65 (1971).
[204] J.-P. Rivera, H. Bill, and R. Lacroix, Phys. Status Solidi A **35**, K105 (1976).
[205] G. Berset, K. Yvon, W. Depmeier, R. Boutellier, and H. Schmid, Ferroelectrics **56**, 13 (1984).